

# Coupled-channel analysis of the $\omega$ -meson production in $\pi N$ and $\gamma N$ reactions for c.m. energies up to 2 GeV. \*

V. Shklyar<sup>†,‡</sup>, H. Lenske, U. Mosel, and G. Penner

*Institut für Theoretische Physik, Universität Giessen, D-35392 Giessen, Germany*

The pion- and photon induced reactions for the final states  $\gamma N$ ,  $\pi N$ ,  $2\pi N$ ,  $\eta N$ , and  $\omega N$  are studied within a coupled-channel effective Lagrangian approach in the energy region from the pion threshold up to 2 GeV. To investigate the role of the nucleon resonances in the different reactions we include all known states with spin- $\frac{1}{2}$ ,  $-\frac{3}{2}$ , and  $-\frac{5}{2}$  and masses below 2 GeV. We find a strong contribution from the  $D_{15}(1675)$  resonance to the  $\pi N \rightarrow \omega N$  reaction. While the  $F_{15}(1680)$  state only slightly influences the  $\omega$  meson production in the  $\pi N$  scattering its role is enhanced in the  $\omega$  photoproduction due to the large electromagnetic coupling of this resonance. We predict the beam asymmetry  $\Sigma_X$  to be a negative in the  $\gamma p \rightarrow \omega p$  reaction near to the threshold. Above the 1.85 GeV the asymmetry is found to change its sign and becomes positive at forward directions. The presented findings can be experimentally tested at GRAAL, CLAS, and CB-ELSA facilities.

PACS numbers: 11.80.-m, 13.75.Gx, 14.20.Gk, 13.30.Gk

## I. INTRODUCTION

The investigation of the pion- and photon-induced reactions on the nucleon in the resonance region is a very interesting and intriguing issue. First, the study of the pion- and photon-nucleon reactions provides very interesting information on the elementary meson-baryon dynamics which is also inevitable input for the investigation of in-medium effects in nuclear matter either in the ground state or at finite temperature. Thus, the information on the  $\omega N$  elastic scattering can not be obtained experimentally, but can, in principle, be extracted from an analysis of the  $(\gamma/\pi)N \rightarrow \omega N$  data provided that all rescattering and threshold effects are carefully treated. This requires a dynamical coupled-channel approach which satisfies the very important condition of unitarity and is constrained by experimental data from all open channels. Secondly, the information on the baryon resonance spectrum can be obtained to distinguish between different quark model predictions and/or lattice QCD results. It is well known that some quark models predict more resonance states than discovered so far (see [1] and references therein). It has been assumed that these 'missing' resonances have small coupling to  $\pi N$  and thereby are not seen in the elastic  $\pi N$  scattering data. Thus, an extensive analysis of other reactions with  $\eta N$ ,  $\omega N$ ,  $K\Lambda$ , and  $K\Sigma$  in the final state is necessary to identify properties of those 'hidden' resonances. With this aim in mind we have developed a coupled-channel effective Lagrangian model [2, 3, 4, 5, 6, 7] that includes the  $\gamma N$ ,  $\pi N$ ,  $2\pi N$ ,  $\eta N$ ,  $\omega N$ ,  $K\Lambda$ , and  $K\Sigma$  final states and is used for simultaneous analysis of all available experimental data in the energy region  $m_N + m_\pi \leq \sqrt{s} \leq 2$  GeV. The premise is to use the same Lagrangians for the pion- and photon-induced reactions, thereby generating the  $u$ - and  $t$ - background contributions without introducing any new parameters. In our last analysis of the pion-induced reactions [8] it has been shown that while the spin- $\frac{5}{2}$  states hardly influence the  $\eta N$ ,  $K\Lambda$ ,  $K\Sigma$  final states, the contributions from  $D_{15}(1675)$  and  $F_{15}(1680)$  to  $\pi N \rightarrow \omega N$  are significant. However, due to the lack of hadronic data it is not possible to draw a firm conclusion about relative resonance couplings to the  $\omega N$  channel until the  $\omega$  meson photoproduction data are included [2, 3].

The  $\omega$  meson photoproduction is under extensive discussion in the literature because of the recently published high precision data from the SAPHIR collaboration [9]. Most of the theoretical studies of this reaction are based on the single channel 'T-matrix' effective Lagrangian calculations [10, 11, 12, 13, 14]. All these findings agree on the importance of the  $t$ -channel  $\pi^0$ -exchange contributions, which has first been studied by Friman and Soyeur [15]. However, some discrepancies exist between the various models on the importance of different resonance contributions to the  $\omega N$  final state. In the quark model of Zhao [11] two resonance states  $P_{13}(1720)$  and  $F_{15}(1680)$  give large contributions to the  $\omega$  meson photoproduction. In the approach of Titov and Lee [14] a resonance part of the reaction is dominated by the  $D_{13}(1520)$  and  $F_{15}(1680)$  states. An opposite observation has been made in the calculation of Y. Oh *et al.* [12] where large contributions to the  $\omega$ -photoproduction come from the 'missing'  $N\frac{3}{2}^+(1910)$  and  $N\frac{3}{2}^-(1960)$

\* Supported by FZ Juelich

<sup>†</sup> On leave from Far Eastern State University, 690600 Vladivostok, Russia

<sup>‡</sup>Electronic address: shklyar@theo.physik.uni-giessen.de

states. In the model of Babacan *et al.* [13] resonance contributions to  $\omega N$  final state have been neglected thereby the reaction process is described by the only nucleon and  $t$ -channel production mechanisms. A good simultaneous description of all available experimental data on the  $(\pi/\gamma)N \rightarrow \omega N$  reactions for  $\sqrt{s} \leq 2$  GeV has been achieved in our previous study [2, 3]. There, strong resonance contributions to these reactions are found to be from the  $P_{11}(1710)$  and  $P_{13}(1900)$  states.

Since all studies predict a different individual resonance contributions to the  $\omega$  photoproduction it is interesting to look at the assumptions made in various models about the resonance couplings to the  $\omega N$  final state. In the approach of Y. Oh *et al.* [12] the  $\omega NN^*$  couplings were introduced by using the quark model predictions from [16, 17]. As a result, only resonances with masses above the  $\omega N$  threshold were taken into account. In the model of Zhao [11] the above problem is solved by using the  $SU(6) \times O(3)$  constituent quark model to also extract contributions from the subthreshold states. However, due to the absence of configuration mixing in this model the contributions from some resonances ( $S_{11}(1650)$ ,  $D_{15}(1675)$ ,  $D_{13}(1700)$ ) are strictly forbidden due to the Moorhouse selection rule [18]. Since the experimentally extracted helicity amplitude  $A_{\frac{1}{2}}^p$  of the  $S_{11}(1535)$  resonance is finite and large this approach was criticized by Titov and Lee in [14]. To overcome this problem these authors perform another study of the  $\gamma p \rightarrow \omega N$  reaction [14] where a vector dominance model (VDM) is used to determine the  $g_{\omega NN}^*$  couplings at the corresponding effective interaction Lagrangians. Therefore, this approach considers only those resonances for which the electromagnetic helicity amplitudes are given in PDG [19]. Another problem with models based on the VDM assumption is that the  $\omega NN^*$  coupling cannot be fully constrained: while the  $A_{1-\frac{1}{2}}^{\omega N}$  and  $A_{1+\frac{3}{2}}^{\omega N}$  helicity amplitudes can be related with the corresponding electromagnetic quantities, an additional assumptions should be put forward to determine  $A_{0+\frac{1}{2}}^{\omega N}$ . Therefore, in the study of [14] the  $\gamma NN^*$  ( $\omega NN^*$ ) dynamics has been simplified by using only one common coupling.

Assuming that some resonances might have small couplings to the  $\pi N$  and  $\gamma N$  final states (see [1, 20]) they can only be excited via rescattering effects in other channels (e.g.  $\eta N$ ,  $\omega N$ , ...). Thus, the use of a coupled-channel approach where all open channel are taken into account is inevitable to identify such resonance contributions. To our knowledge, the only calculation where the  $\omega N$  channel is treated within a coupled-channel approach is a model of Lutz *et al* [21], where point-like interactions are used. There, the lack of the  $J^P = \frac{1}{2}^+$ ,  $J^P = \frac{3}{2}^+$ , and  $J^P = \frac{5}{2}^\pm$  contributions limits the analysis to the near threshold region by assuming  $S$ -wave dominance. There is also a work by Oh and Lee [22, 23] where the authors started to consider rescattering effects from intermediate  $\pi N$  and  $\rho N$  channels.

The Giessen model developed in [2, 3] is based on a unitary coupled-channel effective Lagrangian approach. It has been successfully applied in the analysis of pion- and photon-induced reactions in the energy region up to 2 GeV. In this model the resonance couplings are simultaneously constrained by available experimental data from all open channels. Because of the complexity of the problem, our previous analysis [2, 3] has been restricted to the case of resonances with spin  $J \leq \frac{3}{2}$ . However, the contributions from the spin- $\frac{5}{2}$  resonances to the final states under consideration must be checked explicitly, thus enlarging the model space and increasing the predictive power of the calculations. For example, a strong coupling of  $P_{11}(1710)$  to the  $\omega N$  has been found giving an excess structure in corresponding  $\pi N$  partial wave which is not seen in the SAID group analysis. Since it is not a priory clear, whether spin- $\frac{5}{2}$  couplings to the  $\eta N, \omega N$  etc. can be neglected, the calculations including all possible contributions should be carried out in full. The motivation of this paper is to perform a new combined study of the  $(\gamma/\pi)N$  scattering with  $\gamma N$ ,  $\pi N$ ,  $2\pi N$ ,  $\eta N$ , and  $\omega N$  in the final state where the spin- $\frac{5}{2}$  resonances are included. We check for all resonance contributions in the energy region up to 2 GeV.

Our primary interest is the  $\omega$  meson production. As compared to our previous findings [2, 3] we expect significant changes in the resonant  $\omega$  meson production mechanisms by inclusion of spin- $\frac{5}{2}$  resonance contributions. To provide an additional constraint on the resonance couplings to  $\omega N$  we also include the recent data on the spin density matrix obtained by the SAPHIR group [9]. In Sec. II we briefly outline the main features of the applied model. The calculations of the  $\gamma N \rightarrow \pi N$ ,  $2\pi N$ ,  $\eta N$  reactions and extracted resonance parameters are presented in Sec.III. The results on the  $(\gamma/\pi)N \rightarrow \omega N$  reaction are discussed in Sec. IV and we finish with a Summary.

## II. THE GIESSEN MODEL

The details of the Giessen model can be found in [2, 3, 5, 8]. Here we only outline the main features of the model. The Bether-Salpeter equation (BSE) needs to be solved to obtain the scattering amplitude:

$$\begin{aligned} M(\sqrt{s}, p, p') &= K(\sqrt{s}, p, p') + i \int \frac{d^4 q}{(2\pi)^4} V(\sqrt{s}, p, q) \text{Im} G_{BS}(\sqrt{s}, q) M(\sqrt{s}, q, p'), \\ K(\sqrt{s}, p, p') &= V(\sqrt{s}, p, p') + \int \frac{d^4 q}{(2\pi)^4} V(\sqrt{s}, p, q) \text{Re} G_{BS}(\sqrt{s}, q) M(\sqrt{s}, q, p'), \end{aligned} \quad (1)$$

where the equation is split into the two constituents containing the real and imaginary parts of the propagator  $G_{BS}$ . Here,  $p$  ( $k$ ) and  $p'$  ( $k'$ ) are the incoming and outgoing baryon (meson) four-momenta. To date, a full solution of the equation (1) in the meson-baryon domain only exists for the low-energy  $\pi N$  scattering [24], where no other channels are important. There are many different approximations to the BSE which are mainly three-dimensional reductions (3D) of the original equation. It has been shown that there are an infinite number of ways to perform such a reduction [25] and there is no overwhelming reason to choose one particular approximation over another. Many of these approximations are intended to avoid singularities in the kernel by performing an integration over the relative energy in (1) explicitly. However, due to a technical feasibility, most studies based on 3D approximation are limited to elastic pion-nucleon scattering and there are only a few ones [26, 27] where inelastic channels are also included. To solve the coupled-channel scattering problem with a large number of inelastic channels, we apply the so-called  $K$ -matrix approximation where the real part of the BSE propagator  $G_{BS}$  is neglected. This is the only way which is feasible for the multichannel problem and satisfies the important condition of unitarity.

The imaginary part of the propagator can be written in the form

$$iImG_{BS}(\sqrt{s}, q) = -i\pi^2 \frac{m_{B_q} \sum_{s_B} u(p_q, s_B) \bar{u}(p_q, s_B)}{E_{B_q} E_{M_q}} \delta(k_q^0 - E_{M_q}) \delta(p_q^0 - E_{B_q}), \quad (2)$$

thus, putting intermediate particles on their mass-shells. After the integration over the relative energy, the equation (1) reduces to

$$T_{fi}^{\lambda_f \lambda_i} = K_{fi}^{\lambda_f \lambda_i} + i \int d\Omega_n \sum_n \sum_{\lambda_n} T_{fn}^{\lambda_f \lambda_n} K_{ni}^{\lambda_n \lambda_i}, \quad (3)$$

where  $T_{fi}$  is a scattering matrix and  $\lambda_i(\lambda_f)$  stands for the quantum numbers of initial(final) states  $f, i, n = \gamma N, \pi N, 2\pi N, \eta N, \omega N, K\Lambda, K\Sigma$ . The matrix  $T_{fi}$  is related to  $M$  through  $M = \frac{(4\pi)^2 \sqrt{s}}{\sqrt{pp'm_N m_{N'}}} T_{fi}$  [2]. Using the partial-wave decomposition of  $T, K$  in terms of Wigner functions (see [5]) the angular integration can be easily carried out and the equation is further simplified to the algebraic form

$$T_{fi}^{J\pm, I} = \left[ \frac{K^{J\pm, I}}{1 - iK^{J\pm, I}} \right]_{fi}. \quad (4)$$

The validity of this approximation was demonstrated by Pearce and Jennings in [28] by studying different approximations to the BSE for the  $\pi N$  scattering. Considering different BSE propagators they concluded that an important feature of the reduced intermediate two particle propagator is a delta function on the energy transfer. It has been argued that there is no much difference between physical parameters obtained using the  $K$ -matrix approximation and other schemes. It has also been shown in [29, 30] that for  $\pi N$  and  $\bar{K}N$  scattering the main effect from the off-shell part is a renormalization of couplings and masses. The assumptions made in the  $K$ -matrix approach has been checked by Sato and Lee in their calculations of the pion photoproduction [31]. They find that  $K$ -matrix results are consistent with their dynamical meson-exchange model.

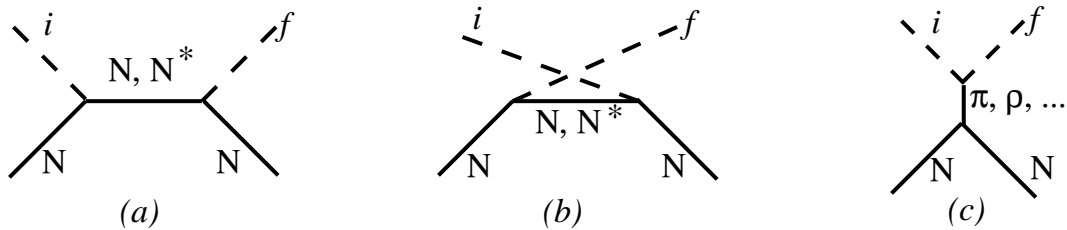
It should be mentioned, however, that within the  $K$ -matrix approach the nature of resonances as three-quark excitations or an outcome of the meson-nucleon dynamics cannot be established. There are findings that, for example, the Roper  $P_{11}(1440)$  resonance might be a quasibound  $\sigma N$ -state [32, 33, 34]. There are also studies based on the chiral model calculations where the  $S_{11}(1535)$  resonance is dynamically generated in the  $K\Sigma$  and  $\eta N$  channels [35, 36]. Since in the  $K$ -matrix approach the real part of  $G_{BS}$  is neglected such resonances cannot appear as a quasibound state but have to be included into the potential explicitly. Note, however, that a plain distinction between the three-quark and quasibound pictures is very difficult, if not impossible at all. Such a study may require more extended analysis of experimental data (including electroproduction data) where information on the spatial content of the resonances can be obtained as well.

Due to the smallness of the electromagnetic coupling the photoproduction reactions can be treated perturbatively. This is equivalent to neglecting  $\gamma N$  in the sum over intermediate states  $n$  in (3). Thus, for a photoproduction process the equation (4) can be rewritten as follows

$$T_{f\gamma}^{J\pm, I} = K_{f\gamma}^{J\pm, I} + i \sum_n T_{fn}^{J\pm, I} K_{n\gamma}^{J\pm, I}. \quad (5)$$

In a similar way, the Compton scattering amplitude can be defined as

$$T_{\gamma\gamma}^{J\pm, I} = K_{\gamma\gamma}^{J\pm, I} + i \sum_n T_{\gamma n}^{J\pm, I} K_{n\gamma}^{J\pm, I}. \quad (6)$$

FIG. 1:  $s$ -,  $u$ -, and  $t$ - channel contributions to the interaction potential.

	mass [GeV]	$J^P$	$I$	reaction
$\pi$	0.138	$0^-$	1	$(\gamma, \gamma), (\gamma, \pi), (\gamma, \omega)$
$\eta$	0.547	$0^-$	0	$(\gamma, \gamma), (\gamma, \omega)$
$\omega$	0.783	$1^-$	0	$(\gamma, \pi), (\gamma, \eta)$
$\sigma$	0.650	$0^+$	0	$(\pi, \pi)$
$f_2$	1.270	$2^+$	0	$(\pi, \pi)$
$\rho$	0.769	$1^-$	1	$(\pi, \pi), (\pi, \omega), (\gamma, \pi), (\gamma, \eta)$
$a_0$	0.983	$0^+$	1	$(\pi, \eta)$

TABLE I: Properties of mesons which give contributions to different reactions via the  $t$ -channel exchange. The notation  $(\gamma\gamma)$  means  $\gamma N \rightarrow \gamma N$  etc.

In (5,6) summation index  $n$  runs only over hadronic states. With such a treatment of Compton scattering problems with the gauge invariance during the isospin decomposition (see [3]) are avoided. The effects of the intermediate  $\gamma N$  states have been checked in [3] and found to be negligible.

### A. K-matrix

The interaction potential ( $K$ -matrix) of the BSE is built up as a sum of  $s$ -,  $u$ -, and  $t$ -channel contributions corresponding to the tree level Feynman diagram shown in Fig. (1). Thus, the resonance and background contributions are consistently generated from the same effective interaction Lagrangians. The Lagrangians used to construct the interaction potential are given in Appendix A and are discussed in [2, 3, 5, 8]. The  $t$ -channel contributions to the different final states are summarized in Table I. Using the interaction Lagrangians and values of the corresponding meson decay widths taken from PDG [19] the following hadronic coupling constant are obtained:

$$\begin{aligned}
 g_{\rho\pi\pi} &= 6.020, & g_{\omega\rho\pi} &= 2.060, \\
 g_{a_0\eta\pi} &= -2.100, & g_{f_2\pi\pi} &= 5.760, \\
 g_{\rho\pi\gamma} &= 0.105, & g_{\rho\eta\gamma} &= -0.928, \\
 g_{\omega\pi\gamma} &= 0.313, & g_{\omega\eta\gamma} &= -0.313, \\
 g_{\pi\gamma\gamma} &= 0.037, & g_{\eta\gamma\gamma} &= 0.142.
 \end{aligned} \tag{7}$$

All other coupling constants are allowed to be varied during the fit. To take into account the finite size of mesons and baryons each vertex is dressed by a corresponding form factor:

$$F_p(q^2, m^2) = \frac{\Lambda^4}{\Lambda^4 + (q^2 - m^2)^2}. \tag{8}$$

Here  $q$  is a c.m. four momentum of an intermediate particle and  $\Lambda$  is a cutoff parameter. It has been shown in [2, 3] that Eq. (8) gives systematically better results therefore we do not use any other forms for  $F(q^2)$ . The cutoffs  $\Lambda$  in (8) are treated as free parameters being varied during the calculation. However, we demand the same cutoffs in all channels for a given resonance spin  $J$ :  $\Lambda_{\pi N}^J = \Lambda_{\pi\pi N}^J = \Lambda_{\eta N}^J = \dots$  etc., ( $J = \frac{1}{2}, \frac{3}{2}, \frac{5}{2}$ ). This greatly reduces the number of free parameters; i.e. for all spin- $\frac{5}{2}$  resonances there is only one cutoff  $\Lambda = \Lambda_{\frac{5}{2}}$  for all decay channels.

The use of vertex form factors requires for a special care on preserving the gauge invariance when the Born contributions to photoproduction reactions are considered. Since the resonance and intermediate meson vertices are

$g$	value	$g$	value
$g_{NN\pi}$	12.85	$g_{NN\sigma} \cdot g_{\sigma\pi\pi}$	36.01
	12.85		22.92
$g_{NN\rho}$	4.40	$\kappa_{NN\rho}$	2.33
	4.53		1.47
$g_{NN\eta}$	0.41	$g_{NNa_0}$	-69.70
	0.10		-70.60
$g_{NN\omega}$	4.19	$\kappa_{NN\omega}$	-0.79
	3.94		-0.94
$g_{NNf_2}$	5.75	$h_{NNf_2}$	-10.87
	—		—

TABLE II: Nucleon and  $t$ -channel couplings obtained in the present study (first line) vs. the results from [2, 3](second line).

gauge invariant they can be independently multiplied by the corresponding form factors. For the nucleon contributions to a meson photoproduction we apply the suggestion of Davidson and Workman [37] and use the crossing symmetric common form factor:

$$\tilde{F}(s, u, t) = F(s) + F(u) + F(t) - F(s)F(u) - F(s)F(t) - F(u)F(t) + F(s)F(u)F(t). \quad (9)$$

At present, the inelastic  $2\pi N$  channel is described by means of an effective  $\zeta N$  state where  $\zeta$  is an effective isovector meson with mass  $m_\zeta = 2m_\pi$ . We allow only resonance coupling to  $\zeta N$  therefore the decay  $N^* \rightarrow \zeta N$  represents a total resonance flux to the  $\rho N, \pi\Delta, \sigma N$  final states. To constrain contributions to this channel we use as an input data the inelastic  $2\pi N$  partial wave cross sections extracted by Manley *et al.* [38]. In our previous studies [2, 3] it has been shown that a good description of the  $2\pi N$  channel is possible and inelastic data are well reproduced. Thus, in the present calculations we continue to use this simplified description of the  $2\pi N$  channel keeping in mind that for a more reliable description of this channel a decomposition of the  $2\pi N$  final state into intermediate  $\rho N, \pi\Delta, \sigma N$  (similar to [39, 40]) is desirable.

### B. $t$ -channel and Born contributions

The extracted  $t$ -channel and Born couplings are shown in Table II. The obtained  $g_{\pi NN}=12.85$  is slightly lower than found in other analysis, for example by SAID group [41, 42]:  $g_{\pi NN}=13.13$ . Note, however, that the present calculation examines a large energy region using only one  $\pi NN$  coupling constant, thereby putting large constraints through all production channels on this coupling and the threshold region only plays a minor role. For example, the  $\pi NN$  coupling is especially influenced by the  $t$ -channel pion exchange mechanism of the  $\omega N$  photoproduction, which is due to the restriction of using only one cutoff value  $\Lambda_t$  for all  $t$ -channel diagrams.

The  $\eta NN$  coupling is found to be small. This corroborates our previous findings [2, 3, 6, 7] and the results from [43, 44]. Compared to [2, 3] also the contribution from the  $f_2(1270)$  meson exchange is taken into account. This produces an additional background leading to a change of the  $g_{NN\sigma} \cdot g_{\sigma\pi\pi}$  coupling constant which appears to be larger than in the previous calculations, see Table II.

Since each interaction vertex is dressed by a form factor (8), special care should be taken when the values from Table II are compared to results from other calculations. Thus, we obtain a smaller value for the  $g_{NN\omega}=4.19$  coupling constant as compared to e.g.  $g_{NN\omega}=15.9$  derived in the Bonn model for the nucleon-nucleon scattering [45]. However, it has been stressed, that taking relativistic effects into account requires the reduce of  $g_{NN\omega}$  in the  $NN$  interaction [46]. Moreover, in the  $NN$  scattering the  $\omega NN$  coupling is utilized to describe the  $t$ -channel exchange thereby its contribution is modified by a form factor. Therefore, the actual values can be used only in combination with the attached form factor and in the kinematical region where they have been applied to. Thus, in the model of Titov and Lee [14] the value  $g_{\pi NN}=10.35$  is used with the form factor of the same shape as in Eq. (8). However, due to the small cutoff values  $\Lambda_\omega=0.5$  applied in [14] the contribution from the corresponding Born term is considerably suppressed.

$\Lambda_N$ [GeV]	$\Lambda_{\frac{1}{2}}^h$ [GeV]	$\Lambda_{\frac{3}{2}}^h$ [GeV]	$\Lambda_{\frac{5}{2}}^h$ [GeV]	$\Lambda_{\frac{1}{2}}^\gamma$ [GeV]	$\Lambda_{\frac{3}{2}}^\gamma$ [GeV]	$\Lambda_{\frac{5}{2}}^\gamma$ [GeV]	$\Lambda_t^{h,\gamma}$ [GeV]
0.952	3.80	0.970	1.13	1.67	4.20	1.167	0.77
0.960	4.30	0.960	—	1.69	4.30	—	0.70

TABLE III: Cutoff values for the form factors (first line) in comparison with the previous global results from [3] (second line). The lower index denotes the intermediate particle, i.e.  $N$ : nucleon,  $\frac{1}{2}$ : spin- $\frac{1}{2}$  resonance,  $\frac{3}{2}$ : spin- $\frac{3}{2}$ ,  $\frac{5}{2}$ : spin- $\frac{5}{2}$  resonance,  $t$ :  $t$ -channel meson. The upper index  $h(\gamma)$  denotes whether the value is applied to a hadronic or electromagnetic vertex.

### III. FIXING THE RESONANCE PARAMETERS

In our calculations we included the following 11 isospin  $I = \frac{1}{2}$  resonances:  $P_{11}(1440)$ ,  $D_{13}(1520)$ ,  $S_{11}(1535)$ ,  $S_{11}(1650)$ ,  $D_{15}(1675)$ ,  $F_{15}(1680)$ ,  $P_{11}(1710)$ ,  $P_{13}(1720)$ ,  $P_{13}(1900)$ ,  $F_{15}(2000)$ , and  $D_{13}(1950)$ , which is denoted as  $D_{13}(2080)$  by the PDG [19]. Thus, contributions from all important resonance states in the energy region from the pion threshold up to 2 GeV are taken into account.

In this energy range only  $N_{17}(1990)^*$  is not included because this resonance has very large mass close to the upper energy limit of our model. Thus, the contribution from this state is expected to be small.

Since the resonant part of the  $\omega$  meson production amplitude is proportional to the two coupling constants  $g_{(\gamma/\pi)NN^*}g_{\omega NN^*}$  the resonance couplings  $g_{\gamma NN^*}$  and  $g_{\pi NN^*}$  are needed to be fixed first. Taking the best hadronic result from [8] we perform a new coupled-channel calculation of the pion- and photon-induced reactions in the region up to 2 GeV where free coupling constants are constrained by full set of experimental data in the  $\gamma N$ ,  $\pi N$ ,  $2\pi N$ ,  $\eta N$ ,  $K\Lambda$ ,  $K\Sigma$ , and  $\omega N$  channels. We obtain a significantly improved  $\chi^2$  for the photon induced reactions with  $\omega N$ ,  $K\Lambda$ , and  $K\Sigma$  in the final states:  $\chi^2=4.2(6.25)$ ,  $2.1(3.95)$ ,  $1.6(2.74)$  respectively, where the values from our previous results are shown in brackets. For other channels the resulting  $\chi^2$  are very similar to the values from the best global fit in [2, 3]. As pointed out before, in this paper we concentrate on the  $\omega$  meson production. The results on the associated strangeness production are presented in [47]. First, we briefly discuss the results on the  $\pi N$  and  $2\pi N$  channels.

#### A. $\pi N$ final state

The results for the elastic  $\pi N$  partial wave amplitudes with isospin  $I = \frac{1}{2}$  in comparison with our previous findings from [2] are shown in Fig. (2). The calculated total  $2\pi N$  partial wave cross sections and corresponding  $\pi N$  inelasticities are presented in Fig. (3). Note, that the  $\pi N$  inelasticities are not fitted but obtained as a sum of the individual contributions from all open channels.

Since the SAID multipole data have rather small error bars and but scatter a lot the description of the pion-photoproduction multipoles turns out to be a difficult task. The calculated multipoles are shown in Figs. (4,5) in comparison with the energy-independent SAID solution [49]. For those energy region where the single-energy results were absent, the gaps were filled by the energy-dependent solution of the SAID group.

There are two resonances  $S_{11}(1535)$  and  $S_{11}(1650)$  which are necessary to describe the  $S_{11}$  partial wave. In order to describe the second resonance peak at  $\sqrt{s}=1650$  MeV in the  $E_{0+}^p$  multipole the fit shifts the mass of  $S_{11}(1650)$  to the lower value 1661 MeV. This leads to a somewhat worse description of the  $S_{11}$  partial wave in the second resonance region, see Fig. (2). In the analyses [39, 40, 50] a third resonance  $S_{11}(2090)$  has been identified below 2 GeV. Moreover, in the model of Chen et al. [51], a fourth  $S_{11}$  resonance has been found above 2 GeV. We have also checked whether the inclusion of a third resonance would improve the results. However, the fit gives zero width for this resonance thereby we do not find any support for this state in the present calculations.

The inclusion of spin- $\frac{5}{2}$  resonance contributions greatly changes the  $\omega$  meson production mechanism. Through the coupled-channel effects, the change in the  $\omega N$  channel affects other reactions which is also seen in the  $\pi N$  partial waves, Fig. (2). In the present study we find minor contributions from the  $P_{11}$  resonances to the  $\omega N$  final state thereby a kink structure at  $\sqrt{s}=1.72$  GeV is not visible any more in the  $P_{11}$  partial wave, see Section IV. This is in line with the results of the SAID analysis [48] which show an almost flat behaviour in this energy region. There are only minor changings in other partial waves as compared to our previous calculations.

For the mass and width of the Roper resonance we find  $M = 1517$  MeV and  $\Gamma = 608$  MeV which turn out to be rather large in comparison with results from other studies, see Table IV. However, the baryon analysis of Vrana et al. [40] give  $490\pm 120$  MeV for the total width. There are also calculations of Cutkosky and Wang [52] where a width of 661 and 545 MeV have been extracted from the analysis of the  $\pi N$  and  $2\pi N$  data. The properties of the  $P_{11}(1440)$  are found to be very sensitive to the background contributions, i.e. to the interference pattern between nucleon and

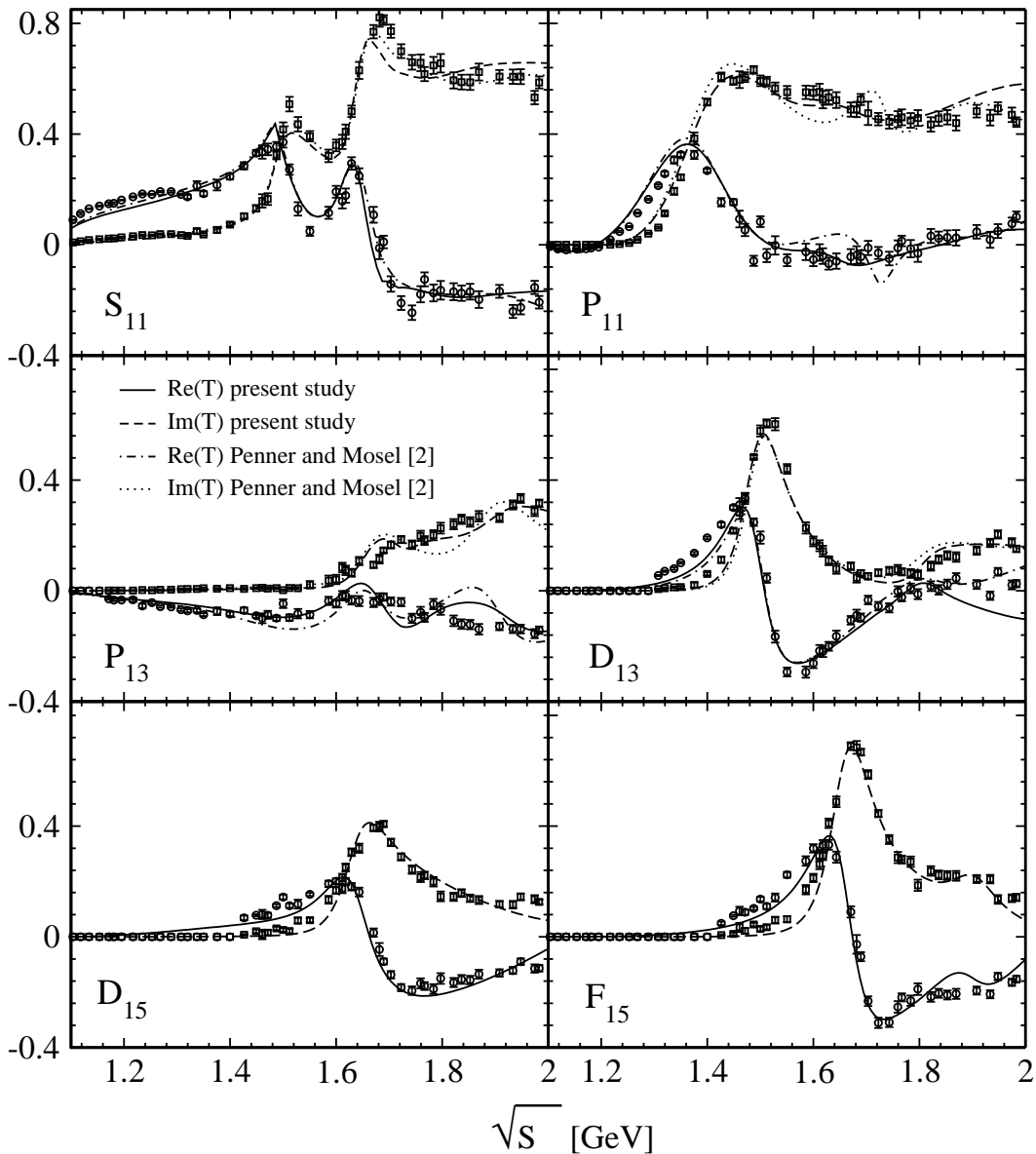


FIG. 2:  $\pi N \rightarrow \pi N$  elastic partial waves for  $I=\frac{1}{2}$ . The solid (dashed) lines corresponds to the real (imaginary) part of the amplitude. Our previous best global results from [2] are shown by the dash-dotted and dotted lines. The data are taken from the SAID analysis [48].

the  $t$ -channel  $\rho$ -meson exchange. Since the description of the  $E_{0+}^{p/n}$  multipole requires a rather soft nucleon cutoff (see Table (III)), the description of the  $S_{11}$  and  $P_{11}$  wave becomes worse. The fit tried to compensate this effect by enlarging the mass and width of  $P_{11}(1440)$ . Note, however, that the  $\pi N$  and  $2\pi N$  branching ratios of  $P_{11}(1440)$  are found to be consistent with the result from other analysis, see Table IV. We find a second state  $P_{11}(1710)$  which is completely inelastic and has a very small branching ratio to  $R_{\pi N}$  as required by the SAID data. However, the decrease in  $\pi N$  coupling of this resonance is compensated by the increase of the  $R_{2\pi N}$  and  $R_{\eta N}$  keeping the production  $R_{\pi N} \cdot R_{2\pi N}$  and  $R_{\pi N} \cdot R_{\eta N}$  in line with the results from our previous global fit [2, 3]. Hence a good description of the  $2\pi N$  cross section and  $\pi N$  inelasticity is possible, see Fig. (3). Note, that the vanishing  $\pi N$  decay width of this resonance is also found by the SAID group [48].

The  $P_{13}$  inelasticity from the SAID analysis [48] in the energy region between 1.55 and 1.7 GeV increases up to 4 mb while the  $2\pi N$  cross section extracted by Manley et al. [38] is found to be zero, see Fig. (3). This might be an indication that either the extracted  $2\pi N$  cross section is inconsistent with the SAID data or another inelastic channel

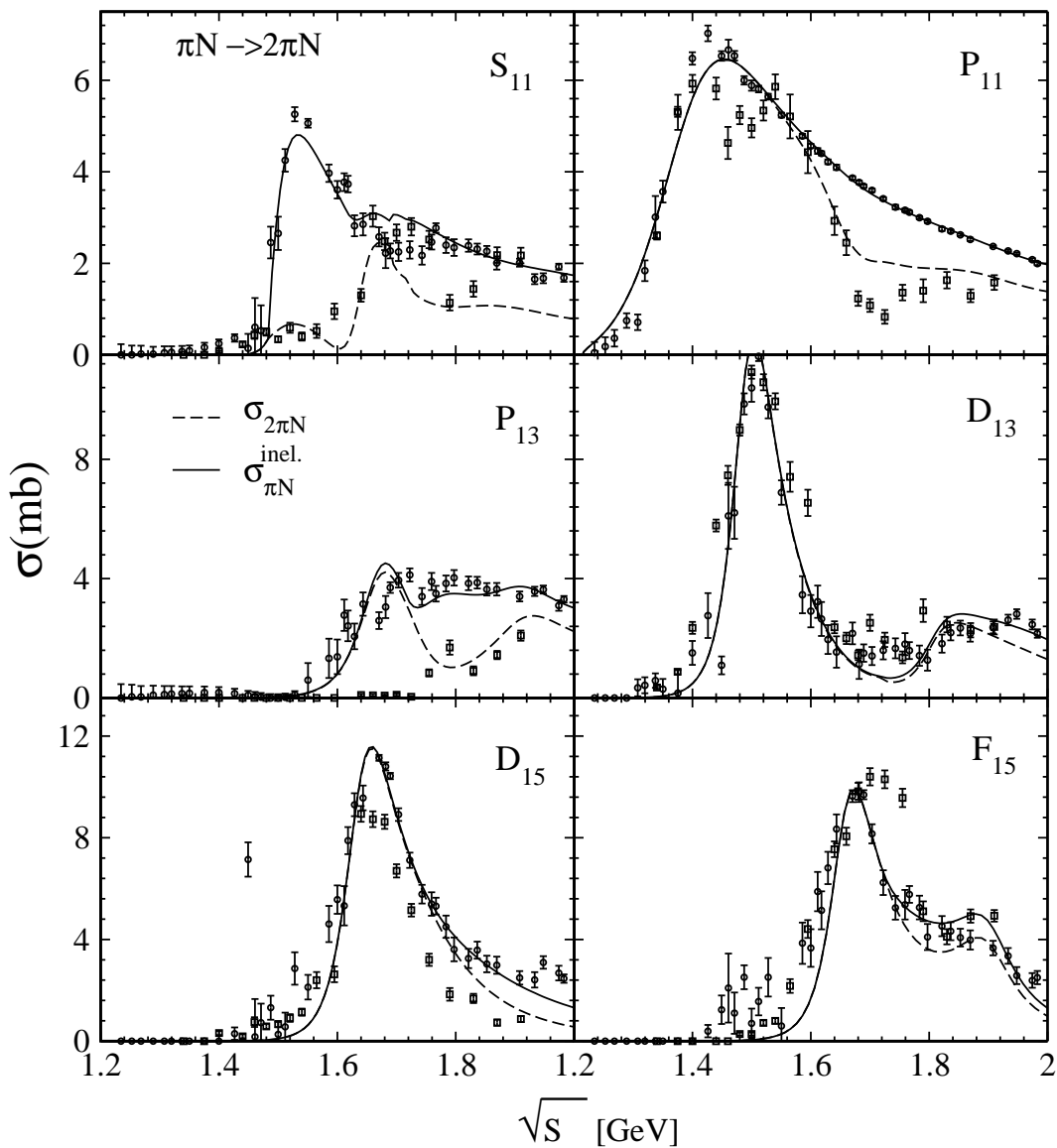


FIG. 3:  $\pi N \rightarrow 2\pi N$  total partial wave cross sections and  $\pi N$  inelasticities for  $I=\frac{1}{2}$ . The solid (dashed) lines corresponds to  $\sigma_{\pi N}^{inel.}$  ( $\sigma_{2\pi N}$ ). The data are taken from [38, 48].

(not  $2\pi N$ ) gives noticeable contributions to this partial wave. The same problem has also been reported by Manley and Saleski in their combined analysis of the  $\pi N \rightarrow \pi N$  and  $\pi N \rightarrow 2\pi N$  reactions [39]. These authors suggested that the discrepancy between the data can be related with the inelastic contributions from the  $3\pi N$  final state. So far, no analysis has been made to describe, e.g., the  $\rho\Delta$  channel. Therefore, we follow [39] and increase the error bars of the original  $2\pi N$  data to prevent the calculations from putting much weight to this discrepancy.

There are two resonances  $P_{13}(1720)$  and  $P_{13}(1900)$  which contribute to the  $P_{13}$  partial wave. The properties of the first resonance are not well fixed: Manley and Saleski [39] give for the total width  $383 \pm 179$  MeV while in the analysis of Vrana et al. [40] the another value of  $121 \pm 39$  MeV has been extracted. We obtain  $\Gamma = 152$  MeV which is close to the results of [40]. The second resonance  $P_{13}(1900)$  is rated by PDG by two stars and was only found in the calculations of Manley and Saleski [39]. We also find a necessity of the inclusion of this resonance to describe the  $P_{13}$  partial wave data, see Fig. (2). However, only a satisfactory description of the real part of the  $E_{1+}^P$  multipole in the energy region between 1.5 and 2 MeV is still possible, see Fig. (4). This problem is due to a missing background contributions to  $E_{1+}^P$ . Since the problem starts at the same energy where the discrepancy between the SAID inelasticity and the  $2\pi N$  cross section in the  $P_{13}$  partial wave is observed, it might be also related to the lack of the  $3\pi N$  contributions

$L_{2I,2S}$	mass	$\Gamma_{tot}$	$R_{\pi N}$	$R_{2\pi N}$	$R_{\eta N}$	$R_{\omega N}$	$g_{RN\omega}^1$	$g_{RN\omega}^2$	$g_{RN\omega}^3$
$S_{11}(1535)$	1526	136	34.4	9.5(+)	56.1(+)	—	3.79	6.50	—
	1534(7)	151(27)	51(5)						
	1542(3)	112(19)	35(8)		51(5)				
$S_{11}(1650)$	1664	131	72.4	23.1(+)	1.4(-)	—	-1.13	-3.27	—
	1659(9)	173(12)	89(7)						
	1689(12)	202(40)	74(2)		6(1)				
$P_{11}(1440)$	1517	608	56.0	44.0(+)	2.82 <sup>a</sup>	—	1.53	-4.35	—
	1462(10)	391(34)	69(3)						
	1479(80)	490(120)	72(5)		0(1)				
$P_{11}(1710)$	1723	408	1.7	49.8(-)	43.0(+)	0.2	-1.05	10.5	—
	1717(28)	480(230)	9(4)						
	1699(65)	143(100)	27(13)		6(1)				
$P_{13}(1720)$	1700	152	17.1	78.7(+)	0.2(+)	—	-6.82	-5.84	-8.63
	1717 (31)	380(180)	13(5)						
	1716(112)	121(39)	5(5)		4(1)				
$P_{13}(1900)$	1998	404	22.2	59.4(-)	2.5(-)	14.9	5.8	14.8	-9.9
	1879(17)	498(78)	26(6)						
	NF								
$D_{13}(1520)$	1505	100	56.6	43.4(-)	1.2 <sup>b</sup> (+)	—	3.35	4.80	-9.99
	1524(4)	124(8)	59(3)						
	1518(3)	124(4)	63(2)		0(1)				
$D_{13}(1950)$	1934	859	10.5	68.7(+)	0.5(-)	20.1	-10.5	-0.6	17.4
	1804(55)	450(185)	23(3)						
	2003(18)	1070(858)	13(3)		0(2)				
$D_{15}(1675)$	1666	148	41.1	58.5(+)	0.3(+)	—	109	-99.00	83.5
	1676(2)	159(7)	47(2)						
	1685(4)	131(10)	35(1)		0(1)				
$F_{15}(1680)$	1676	115	68.3	31.6(+)	0.0(+)	—	12.40	-35.99	-78.28
	1684(4)	139(8)	70(3)						
	1679(3)	128(9)	69(2)		0(1)				
$F_{15}(2000)$	1946	198	9.9	87.2(-)	2.0(-)	0.4	-19.6	19.3	23.14
	1903(87)	490(310)	8(5)						
	NF								

TABLE IV: Properties of  $I = \frac{1}{2}$  resonances extracted in the present study (1st line) in comparison with the values from [39] (2nd line), and [40] (3th line). In brackets, the estimated errors are given. The mass and total width are given in MeV, the decay ratios in percent. <sup>b</sup>: The decay ratio is given in 0.1‰.

to this channel [3] as discussed above. Therefore, it would be desirable to account for  $3\pi N$  contributions in future investigations.

The mass and width of  $D_{13}(1520)$  extracted in the present calculations are close to values obtained by Arndt et al. [41, 49]:  $1516 \pm 10$  and  $106 \pm 6$  MeV correspondingly. Manley and Saleski [39] and Vrana et al. [40] give somewhat larger values, see Table IV. Note, however, that the calculated  $\pi N$  and  $2\pi N$  branching ratios are very close to that of [39, 40]. Apart from the well-established resonance  $D_{13}(1520)$  we also include the second state  $D_{13}(1950)$  which is denoted as  $D_{13}(2080)$  by the PDG [19]. This resonance is poorly established: in all calculations it appears to be almost inelastic and weakly coupled to  $\pi N$ . Despite on its small decay ration to  $\pi N$ , this resonance turns out to be important due to rescattering effects. Without this state the calculations result in considerably worse  $\chi^2$ . The  $D_{13}(1950)$  state is found to be rather broad in the present calculations: the obtained width is about 860 MeV and mass 1934 MeV. Other baryon analysis also identify this state with a large width: Vrana et al. [40] find  $\Gamma = 1070 \pm 858$  MeV and Manley and Saleski [39] obtain  $\Gamma = 447 \pm 185$  MeV. Note, that we do not find any indication for the  $D_{13}(1700)$  resonance

$L_{2I,2S}$	$A_{\frac{1}{2}}^p$	$A_{\frac{1}{2}}^n$	$A_{\frac{3}{2}}^p$	$A_{\frac{3}{2}}^n$
$S_{11}(1535)$	92	-13	—	—
	90(30)	-46(27)	—	—
	60(15)	-20(35)	—	—
$S_{11}(1650)$	57	-25	—	—
	53(16)	-15(21)	—	—
	69(5)	-15(5)	—	—
$P_{11}(1440)$	-84	138	—	—
	-65(4)	40(10)	—	—
	-63(5)	45(15)	—	—
$P_{11}(1710)$	-50	68	—	—
	9(22)	-2(14)	—	—
	7(15)	-2(15)	—	—
$P_{13}(1720)$	-65	1	35	-4
	18(30)	1(15)	-19(20)	-29(61)
	-15(15)	7(15)	7(10)	-5(25)
$P_{13}(1900)$	-8	-19	0	6
	NG			
$D_{13}(1520)$	-13	-70	145	-141
	-24(9)	-59(9)	166(5)	-139(11)
	-38(3)	-48(8)	147(10)	-140(10)
$D_{13}(1950)$	11	40	26	-33
	NG			
$D_{15}(1675)$	9	-56	20	-84
	19(8)	-43(12)	15(8)	-58(13)
	15(10)	-49(10)	10(7)	-51(10)
$F_{15}(1680)$	3	30	115	-48
	-15(6)	29(10)	133(12)	-33(9)
	-10(4)	30(5)	145(5)	-40(15)
$F_{15}(2000)$	10	9	25	-4
	NG			

TABLE V: Helicity decay amplitudes of  $I = \frac{1}{2}$  resonances ( in  $10^{-3} \text{ GeV}^{-\frac{1}{2}}$ ) considered in the present study (first line); second line: values from PDG [19]; third line: results of SAID group [49]; "NG": not given.

contribution in the energy region between 1.7 and 1.9 GeV as compared to results of [39, 40]. In all calculations the fit gives almost zero width for this resonance, hence its contributions vanish.

There is a clear resonance peak in the  $D_{15}$  partial wave, (see Fig. (2)) which corresponds to the  $D_{15}(1675)$  resonance. The comparison of the  $2\pi N$  total cross section extracted by Manley et al. [38] with the SAID inelasticity shown in Fig. (3) reveals the missing inelastic flux of 2 mb around 1.65 GeV. It has been shown in [8] that this flux cannot be absorbed by neither the  $\eta N$ ,  $K\Lambda$ , or  $K\Sigma$  channels. Thus, we conclude that either the  $\pi N$  and  $2\pi N$  data are inconsistent with each other or other open channels (e.g.  $3\pi N$ ) must be taken into account. To overcome this problem and to describe the  $\pi N$  and  $2\pi N$  data in the  $D_{15}$  partial wave the error bars of the original  $2\pi N$  data [38] were weighted by a factor 3. The same procedure was also used by Vrana et al. [40] and Cutkosky et al. [52] to fit the inelastic data. We find an important subthreshold contributions from the  $D_{15}(1675)$  resonance to the  $\pi N \rightarrow \omega N$  reaction, see Section IV. Hence, the  $D_{15}$  inelastic contribution of about 1 mb shifts from the  $2\pi N$  channel to  $\omega N$  above 1.8 GeV as shown in Fig. (3).

Apart from the well established  $F_{15}(1680)$  we also find an indication for the second  $F_{15}(2000)$  resonance to describe the high energy tail of the  $F_{15}$  partial wave amplitude, as seen in Fig. (2) by the shoulder around 1950 MeV. The evidence for this state was also found in earlier works [39, 53]. A visible inconsistency between the inelastic SAID

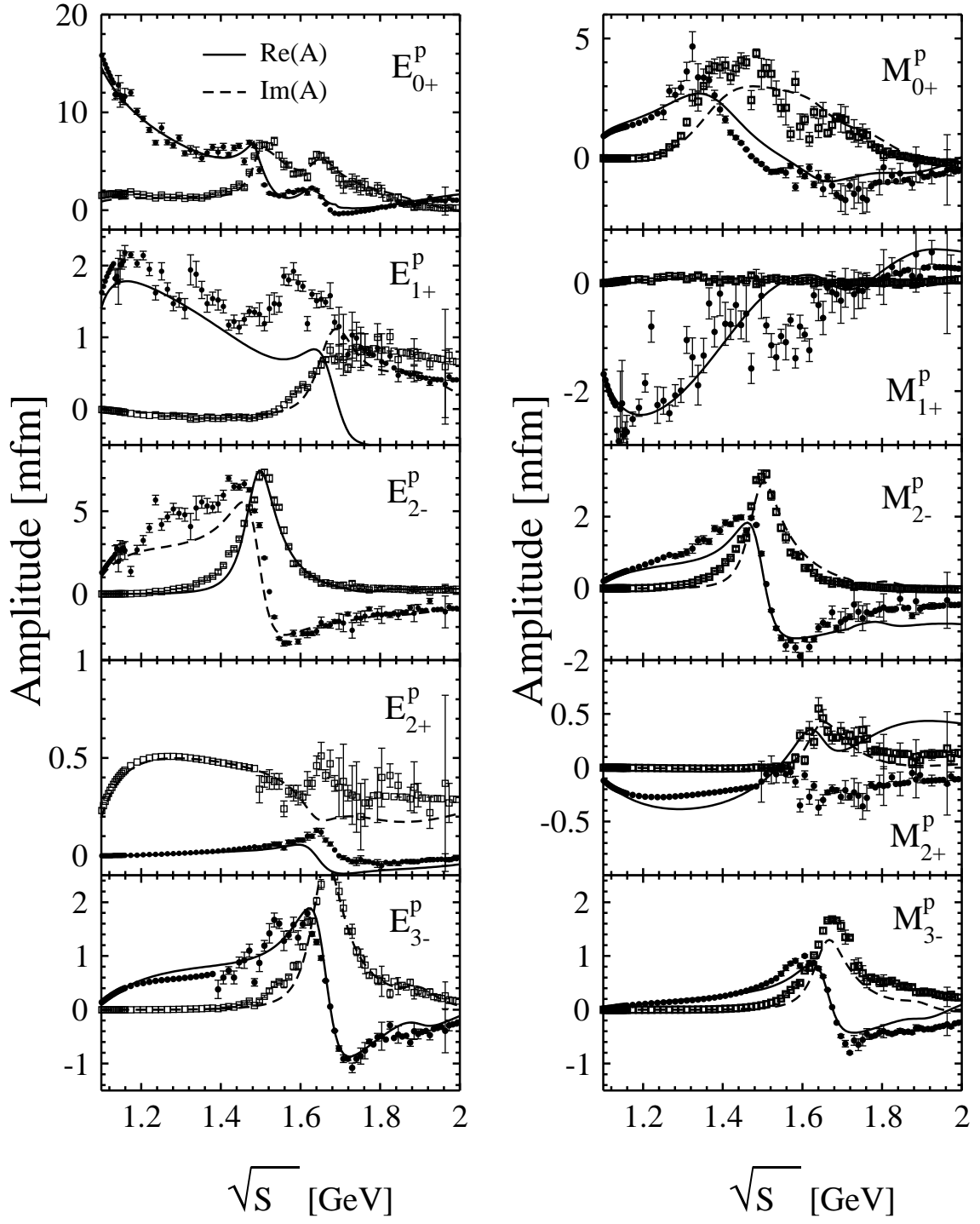


FIG. 4:  $\gamma N \rightarrow \pi N$  proton multipoles. The solid (dashed) line corresponds to the calculated real (imaginary) part of the amplitude. The SAID(SM01) data are taken from [49].

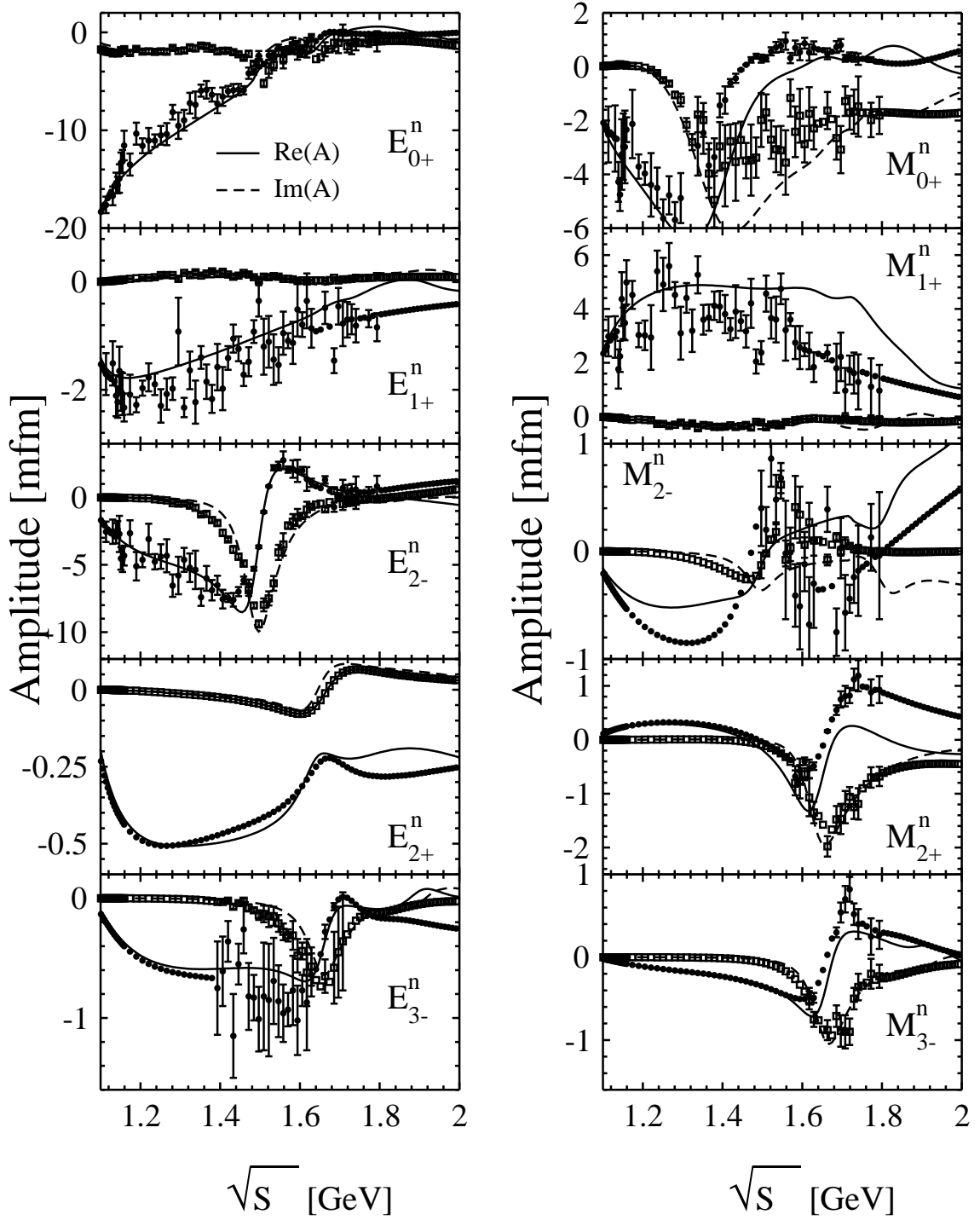


FIG. 5:  $\gamma N \rightarrow \pi N$  neutron multipoles. Notation as in Fig. (4).

data and the  $2\pi N$  cross section from [38] above 1.7 GeV can be seen in  $F_{15}$  wave, see in Fig. 3. The three data points at 1.7, 1.725, and 1.755 GeV are, therefore, excluded from the fitting procedure.

The parameters of the  $D_{15}(1675)$  and  $F_{15}(1680)$  resonances are in line with the results from other groups [19, 39, 40]. The properties of the  $F_{15}(2000)$  state differ strongly in the various analyses: Manley and Saleski [39] give  $490 \pm 310$  MeV for the total decay width while other studies [41, 53] find it at the level of  $95 \div 170$  MeV. Moreover, this state has not been identified in the investigations of [40, 50]. Since the  $F_{15}(2000)$  resonance is found to be strongly inelastic

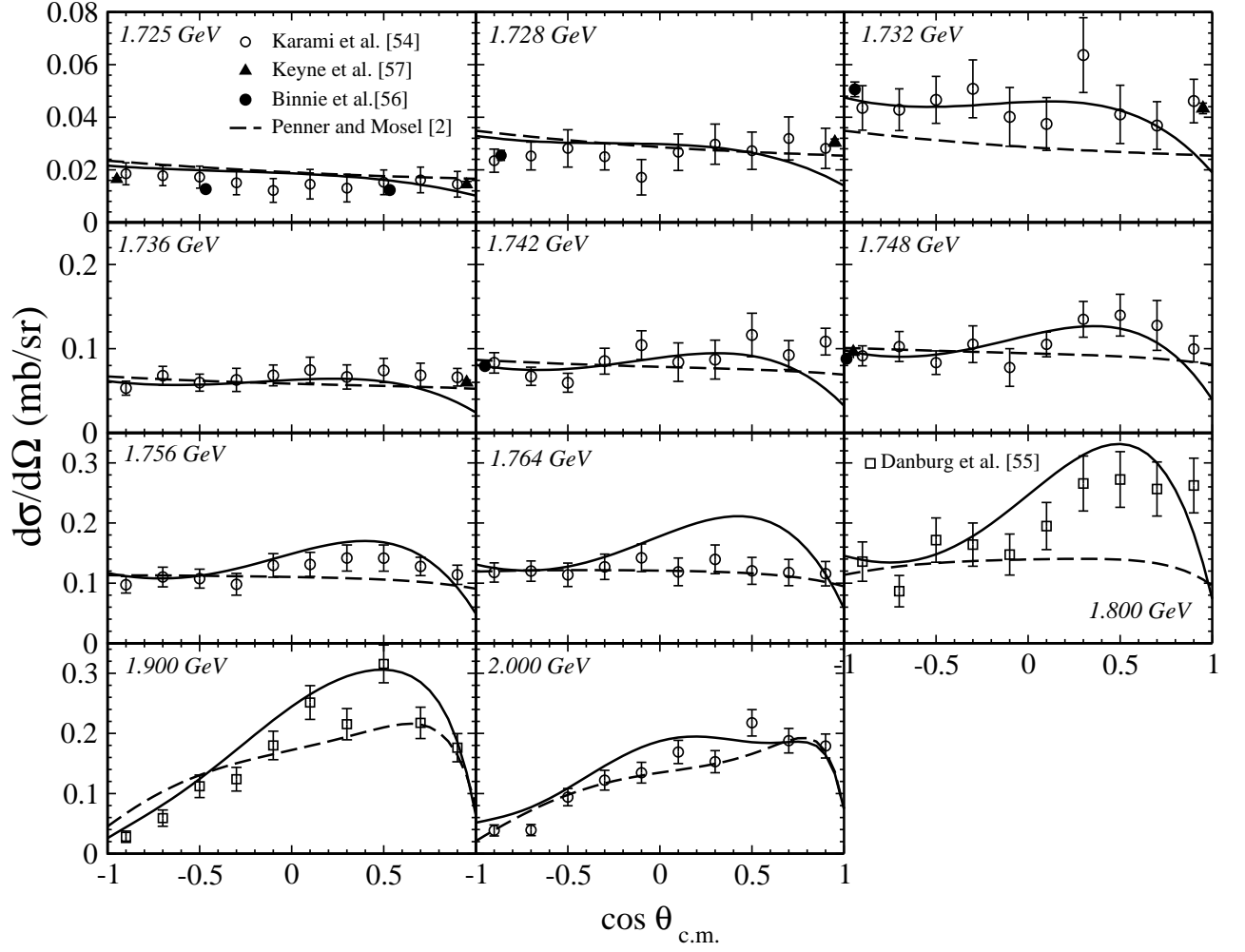


FIG. 6: Differential cross sections of the  $\pi N \rightarrow \omega N$  reaction. The experimental data are taken from [54, 55, 56, 57]. Our previous best global result from [2] is shown by the dashed line.

with 84-88% of inelasticity absorbed by the  $2\pi N$  channel, more  $2\pi N$  data above 1.8 GeV (cf. Fig. 3) are needed for a reliable determination of the properties of this state.

#### IV. RESULTS FOR $\omega$ MESON PRODUCTION

Our main interest is the  $\omega$ -meson production mechanism in the pion- and photon-induced reactions. As pointed out in [2, 3], using only the hadronic data is insufficient to determine the reaction mechanism. Therefore, we carry out a new combined study of the  $\pi N \rightarrow \omega N$  and  $\gamma N \rightarrow \omega N$  reactions in up to 2 GeV energy region. The most significant improvements in the present calculations is the inclusion of the contributions from spin- $\frac{5}{2}$  resonances. In order to constrain the analysis we include the full set of experimentally available informations into the energy region up to 2 GeV. We expect that this extended analysis will provide a much deeper insights into the production mechanism as before. As compared to the previous calculations [2, 3], the additional constraints from the spin density matrix elements of the final  $\omega$  meson measured by SAPHIR are also taken into account.

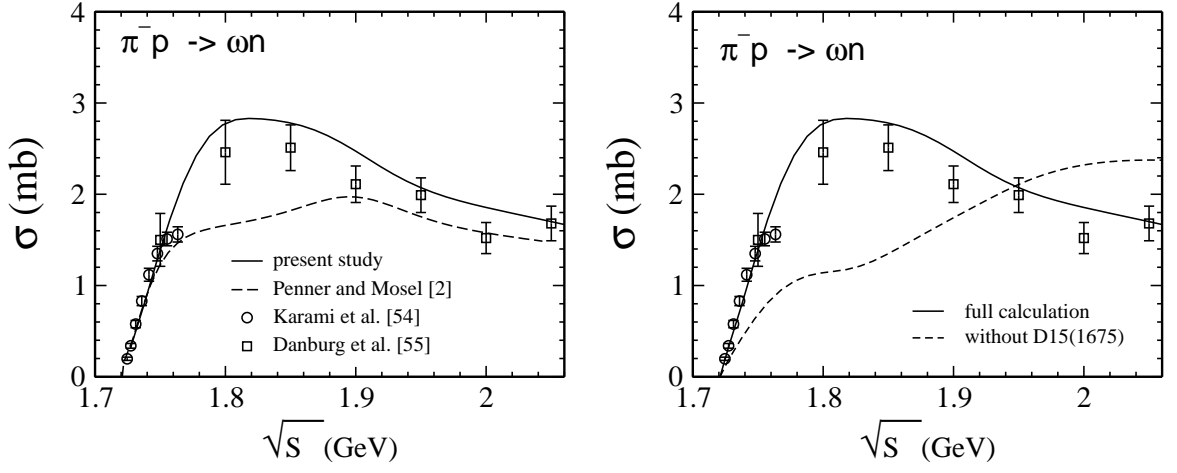


FIG. 7: *Left*: The calculated total  $\pi N \rightarrow \omega N$  cross section in comparison with our previous results from [2]. *Right*: The total cross section calculated with and without the  $D_{15}(1675)$  resonance contributions. The experimental data are taken from [54, 55].

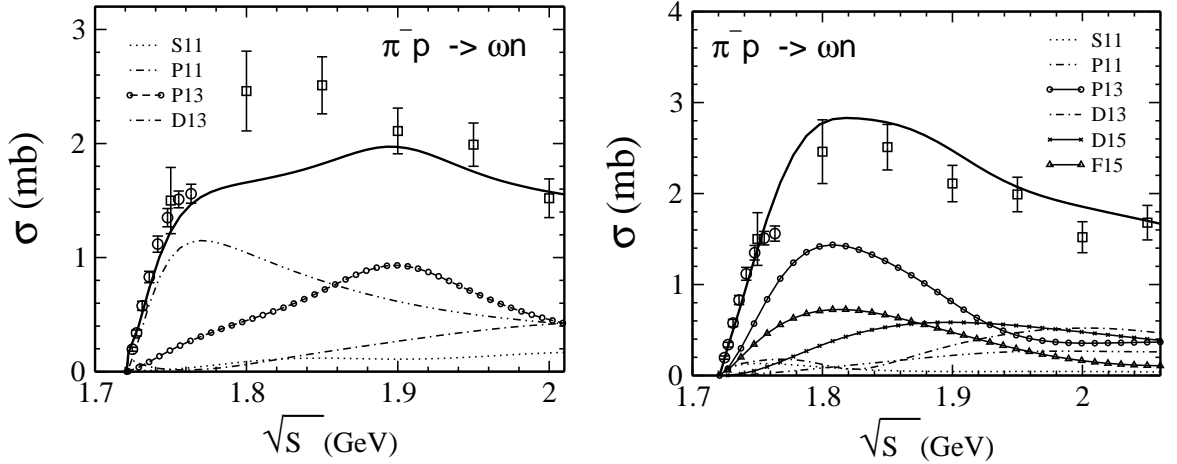


FIG. 8: *Left*: The results of the partial wave decomposition of the total  $\pi N \rightarrow \omega N$  cross section from [2]. *Right*: The partial wave cross sections obtained in the present calculations.

### A. $\pi N \rightarrow \omega N$

All experimental data on the  $\omega$ -meson production in the  $\pi N$  scattering have been measured before 1980 and therefore have rather poor statistics. In total, there are 115 data points which includes differential and total cross sections data. The inclusion of spin- $\frac{5}{2}$  resonance contributions strongly changes the relative resonance contributions to the  $\omega N$  final states in the present calculations, see Fig. (6). In contrast to the findings in [2], the main contributions close to the threshold come from the  $P_{13}$  and  $D_{15}$  partial waves. The resonance part of the production amplitude is dominated by the  $D_{15}(1675)$  state. The result of our calculations without the  $D_{15}(1675)$  contribution is shown in Fig. (7). At the threshold, the reaction mechanism is influenced by the  $S$ -wave contributions leading to a rather flat angular distribution (see Fig. (6)). The major difference between the present calculations and the results from [2] is seen at  $\sqrt{s} = 1.80$  GeV where only the data of Danburg et al. [55] are available. This experimental data shows an increase of the differential cross section at forward angles. In our previous calculations the reaction in this kinematical region is dominated by the  $P_{11}$  wave contributions resulting in a weakly angle dependent differential cross sections. The inclusion of spin- $\frac{5}{2}$  resonances shifts this strength to the  $P_{13}$  and  $D_{15}$  partial waves and the cross section at

$\sqrt{s}=1.80$  GeV follows the Danburg data.

The partial wave decomposition of the  $\pi N \rightarrow \omega N$  reaction is shown in Fig. (8) in comparison with our previous results [2, 3] where the contributions from the spin- $\frac{5}{2}$  resonances have been neglected. Despite of the significant differences in the production mechanisms, we find  $\chi_{\pi\omega}^2 \simeq 1.25$  in both calculations. Thus, the distinction between various results is difficult due to the lack of the hadronic data. However, the results in other channels may be used to constrain the reaction mechanism. In our previous global fit [2, 3], large contributions from the  $P_{11}(1710)$  and  $P_{13}(1900)$  resonances to this reaction have been found. The mass of  $P_{11}(1710)$  ( $M=1752$  MeV) has been found to be above the  $\omega N$  threshold  $M=1.752$  so that this resonance dominated the production cross section from the threshold up to 1.8 GeV. However, such a strong contributions to the  $\omega N$  channel lead to the excess structure in the real and imaginary parts of the  $\pi N$  partial wave amplitude  $P_{11}$  around 1.73 GeV which is not visible by the SAID analysis [48], see Section III A.

We also find strong contributions from the  $P_{13}$  partial wave to the  $\pi N \rightarrow \omega N$  reaction what has been also reported in [2], see Fig. (8). But in contrast to [2], the strength in this partial wave is shifted to the lower energies and becomes more pronounced near to the reaction threshold. The peaking behaviour in the  $P_{13}$  partial cross section is due to the interference pattern between  $P_{13}$  resonances and background contributions to the  $\omega N$  channel. Since the major contributions to the  $\pi N \rightarrow \omega N$  reaction come from the  $P_{13}$  and  $D_{15}$  waves, it is interesting to look at the  $\pi N$  inelasticity for these partial waves. The calculated  $\sigma_{\pi N}^{inel}$  inelasticity in these waves is found to be in line with the SAID data (see Fig. (3)). While the  $P_{13}$  inelastic data are also well described, it would be also desirable to check the obtained results by including contributions from other inelastic ( $3\pi N$ ) channels (see Section (III A)).

### B. $\gamma N \rightarrow \omega N$

The differential  $\omega$  meson photoproduction cross sections are presented in Fig. (9) in comparison with our previous results from [2, 3]. In the present calculations we obtain  $\chi_{\gamma\omega}^2=4.5$  which is significantly better than our previous result ( $\chi_{\gamma\omega}^2=6.25$ ). This improvement strongly supports the extended treatment applied in this work. All studies of this reaction agree on the importance of the  $\pi^0$  exchange reported first by Friman and Soyeur [15]. These contributions lead to the peaking behaviour of the calculated differential cross sections at forward angles which also becomes visible in the SAPHIR measurements [9] above 1.783 GeV, see Fig. (9). More detailed information of the production mechanism is obtained from observables measuring the spin degree of freedom of the  $\omega$  meson. For the  $t$ -channel spinless meson exchange ( $c$ -diagram in Fig. (1)) the spin density matrix  $\rho_{rr'}$  of the final  $\omega$  mesons can be easily calculated, see Appendix B3. In the Gottfried-Jackson frame, where the initial photon and exchange particle are in their rest frame, and  $z$ -axis is in the direction of the incoming photon momentum, the calculation gives  $\rho_{00}^{GJ} = 0$ . On the other hand, the experimental value of  $\rho_{00}^{GJ}$  for forward directions, where the  $\pi^0$  exchange dominates, was measured by SAPHIR and found to be in the range of  $\rho_{00}^{GJ} = 0.2 \dots 0.3$ . Thus, the nonzero matrix element testifies that even in this kinematical region other mechanisms (rescattering effects, interference with resonances) must be important.

There is a visible distinction between results from [3] and present study at energies close to  $\omega N$  threshold, see Fig. (9). Above 1.835 GeV both calculations give similar results and almost coincide at higher energies. However, the differences in the reaction mechanisms can be seen in the partial wave decomposition shown in Fig. (10). We find less contributions from the  $P_{11}$  partial wave as compared to [3]. However, this channel is still important and gives sizeable strength near 1.8 GeV. In contrast to [2, 3], the main contribution at the reaction threshold comes from the  $D_{13}$  partial wave which also leads to the change in the differential cross section behaviour, see Fig. (9). Since the spin- $\frac{5}{2}$  resonances were not included in our previous analysis and at higher energies the cross section was entirely dominated by the background contributions from the partial waves with spin  $J > \frac{3}{2}$ , see Fig. (10), left.

The largest contributions to the  $\omega$  meson photoproduction come from the  $\pi^0$  exchange and the subthreshold spin- $\frac{5}{2}$  resonances:  $D_{15}(1675)$  and  $F_{15}(1680)$ . Since the  $\pi^0$  exchange above 1.8 GeV strongly influences the  $\gamma N \rightarrow \omega N$  reaction a consistent identification of individual resonance contributions from the only partial wave decomposition shown in Fig. (10), right, is difficult. The  $P_{13}(1900)$ , and  $F_{15}(2000)$ , and  $D_{13}(1950)$  states which lie above the reaction threshold hardly influence the reaction due to their small couplings to  $\omega N$ , see Table IV. Despite of the small relative contribution from the  $D_{15}$  and  $F_{15}$  waves to the  $\omega$  photoproduction the cross sections are strongly affected by spin- $\frac{5}{2}$  states because of the destructive interference pattern between the  $\pi^0$  exchange and these resonance contributions, see Fig. (11). The  $D_{13}(1950)$  state has a large branching ratio into the  $\omega N$  final state, see Table IV. However, the contributions from this resonance to the photoproduction are moderate due to its large mass and total width.

While  $F_{15}(1680)$  plays only a minor role in the  $\pi N \rightarrow \omega N$  reaction the contribution from this state becomes more pronounced in the  $\omega$  meson photoproduction because of its large  $A_{\frac{3}{2}}^p$  helicity amplitude, as seen in Table V. The importance of the  $F_{15}(1680)$  resonance to the  $\omega$  meson photoproduction was also found by Titov and Lee [14] and in the model of Zhao [11]. However, in contrast to [14] where also a large effect from  $D_{13}(1520)$  was observed we do not

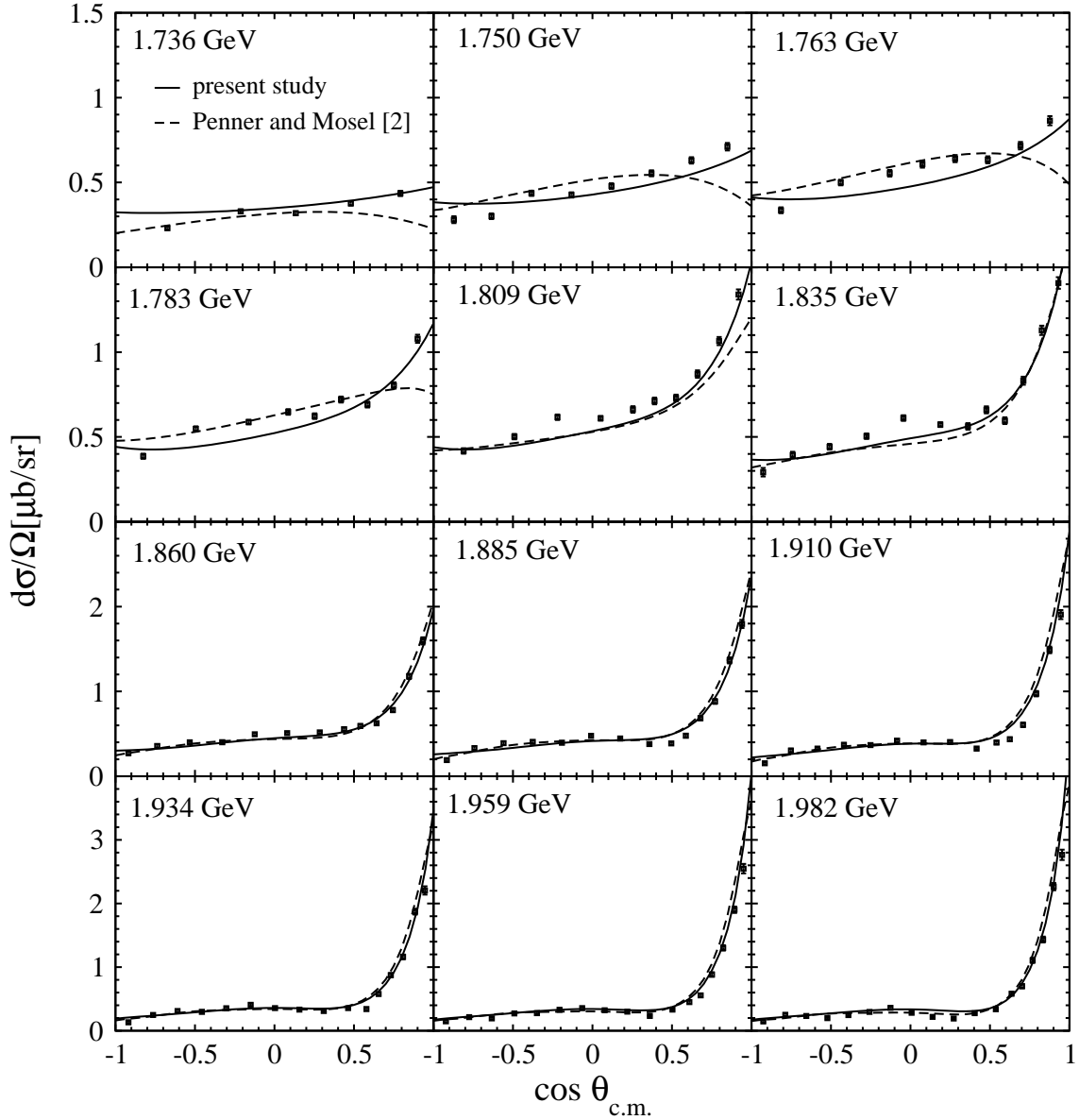


FIG. 9:  $\gamma N \rightarrow \omega N$  differential cross sections in comparison with the SAPHIR data [9] and our previous results from [3].

find any visible contribution from this state. In fact, the strong contribution to the  $D_{13}$  partial wave seen in the right panel of Fig. (10), resembling a resonance structure, comes indeed from non-resonant  $\pi^0$  exchange.

It is interesting to note, that both present study [11, 14] find no significant effect from  $D_{15}(1675)$  state in the  $\omega$  meson photoproduction. Thus, in the quark model of Zhao [11] the contributions from this state is strictly suppressed by the Moorhouse selection rule [18]. While Titov and Lee [14] account for the  $D_{15}(1675) \rightarrow \omega N$  contributions the corresponding  $\omega NN^*$  coupling is determined from the VDM assumptions. Since the electromagnetic helicity amplitudes of this resonance are relatively small, see Table V, the resulting  $\omega NN^*$  coupling also has only marginal effect in this approach.

The  $\rho_{rr'}$  elements extracted from the SAPHIR data [9] are an outcome of the averages over rather wide energy and angle regions, see Fig. (12). Therefore, the original error bars have been decreased by factor 3 to put an additional weight to these data. The inclusion of measured  $\rho_{rr'}$  into the calculations provides a strong additional constraint on the relative partial wave contributions and finally on the resonance couplings. The spin density matrix elements calculated at fixed angles in the helicity frame are presented in Fig. (12). A good description of the spin density matrix is possible in a wide energy region. Since the  $\rho_{rr'}$  data put strong constraints on the  $\gamma p \rightarrow \omega p$  reaction mechanism there is an urgent need for precise measurements of the spin density matrix in more narrow energy bins

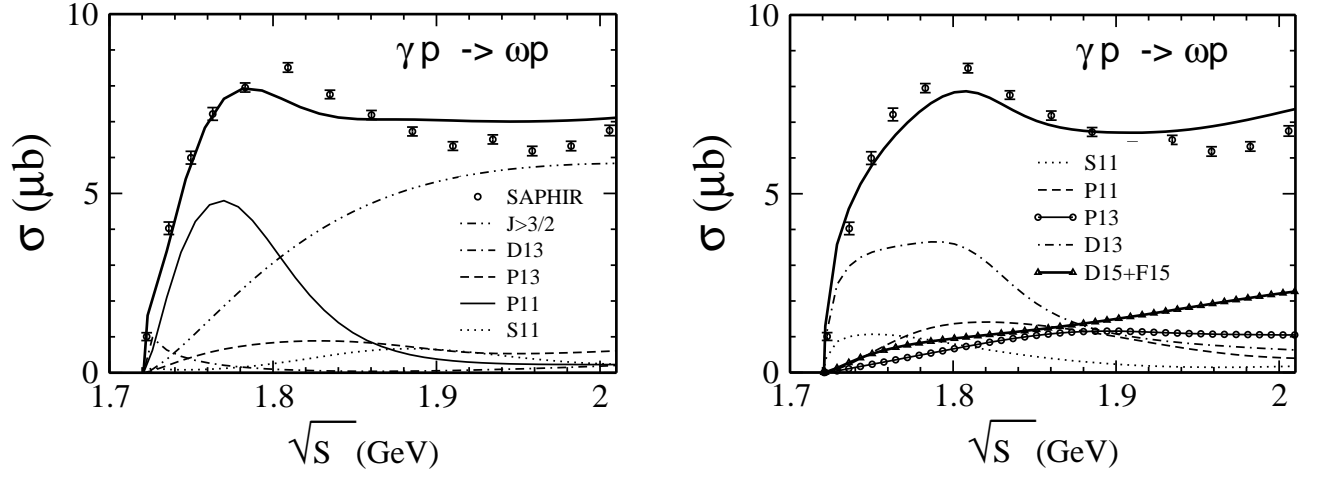


FIG. 10: *Left:* Total and partial wave cross sections from [3]. *Right:* Total and partial wave cross sections calculated in the present study.

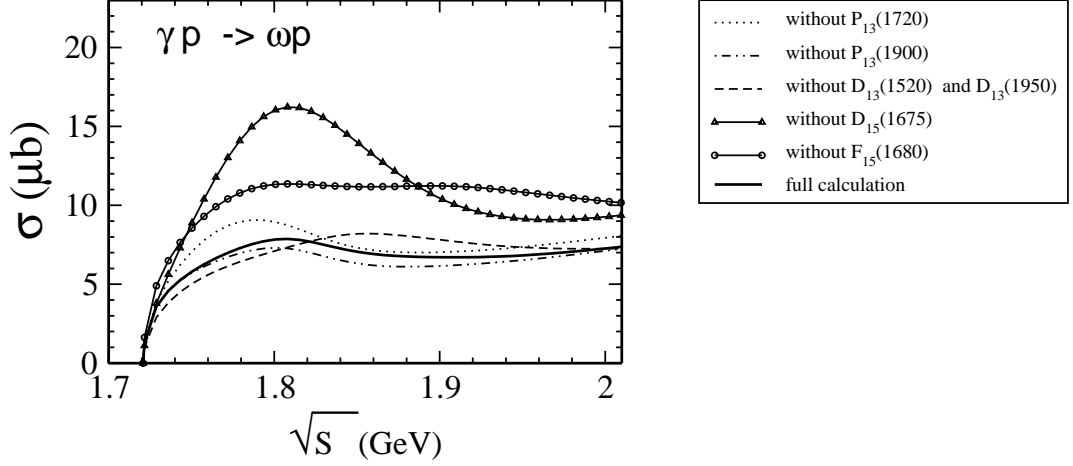


FIG. 11: Role of the individual resonance contributions in the  $\omega$  meson photoproduction.

to pin down the reaction picture.

The calculated photon beam asymmetry  $\Sigma_X$  (see Appendix B 2) is shown in Fig. (13). At energies close to the threshold our calculations predict a negative values of  $\Sigma_X$ . In the energy region between  $1.72 \div 1.8$  GeV the asymmetry has an almost symmetric behaviour. By increasing the c.m. energy the  $\pi^0$  exchange becomes dominant at forward angles leading to a change of the sign at  $\Sigma_X$  above 1.85 GeV. Such a behaviour is especially interesting since it tests an interference pattern between the resonance and background parts of the transition amplitude. The role of this interference becomes more pronounced in the  $\Sigma_A$  and  $\Sigma_B$  asymmetries, see Figs. (14,15). For the pure  $\pi^0$  exchange production mechanism the calculations give  $\Sigma_A=-1$  and  $\Sigma_B=+1$ , see Appendix B 3. Therefore the deviation from these values testifies about magnitude of the interference between the  $\pi^0$  exchange and other production mechanisms. The experimental measurements of these observables provide a good test for the presented model.

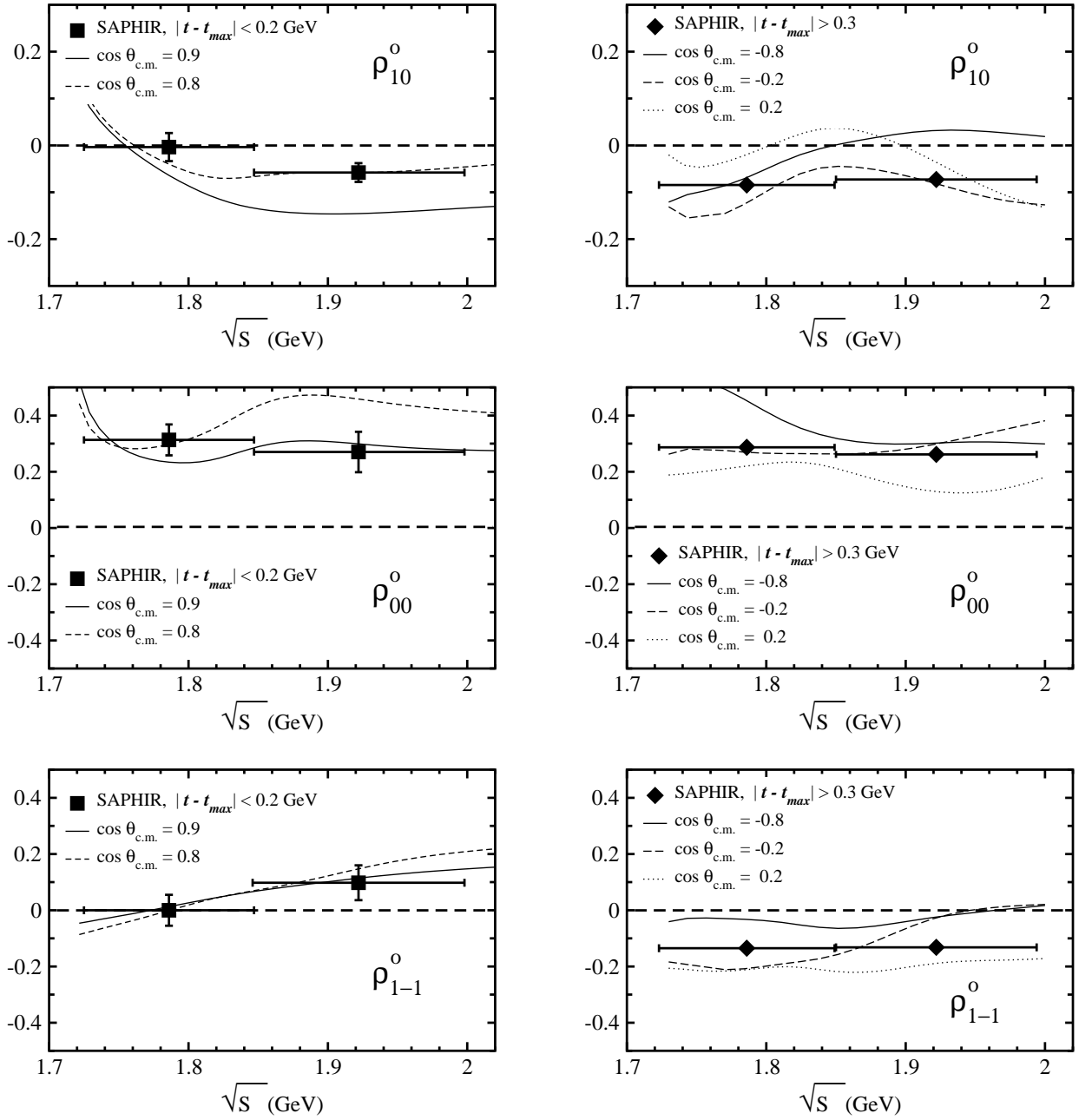


FIG. 12: Spin density matrix elements in the helicity frame in comparison with the SAPHIR measurements [9].

### V. $\omega N$ ELASTIC SCATTERING

In the present calculations this process is completely dominated by the nucleon resonance contributions. The effect of the nucleon Born term is only marginal. The calculated  $\omega N$  elastic total cross section is shown in Fig. (16). The extracted scattering lengths and effective ranges (as defined in Appendix C) are

$$\bar{a} = -0.026 + i0.28, \quad \bar{r} = 6.02 + i0.062. \quad (10)$$

The result for  $Im\bar{a}=0.28$  fm is consistent with values obtained by Lutz et al. [21]  $\bar{a} = -0.44 + i0.20$  fm and Klingl and Weise [58]  $a = 1.6 + i0.30$  fm. Note, however that calculated scattering lengths (10) should be taken with care since the present calculations are not concentrated on the description of the near to threshold region but consider a

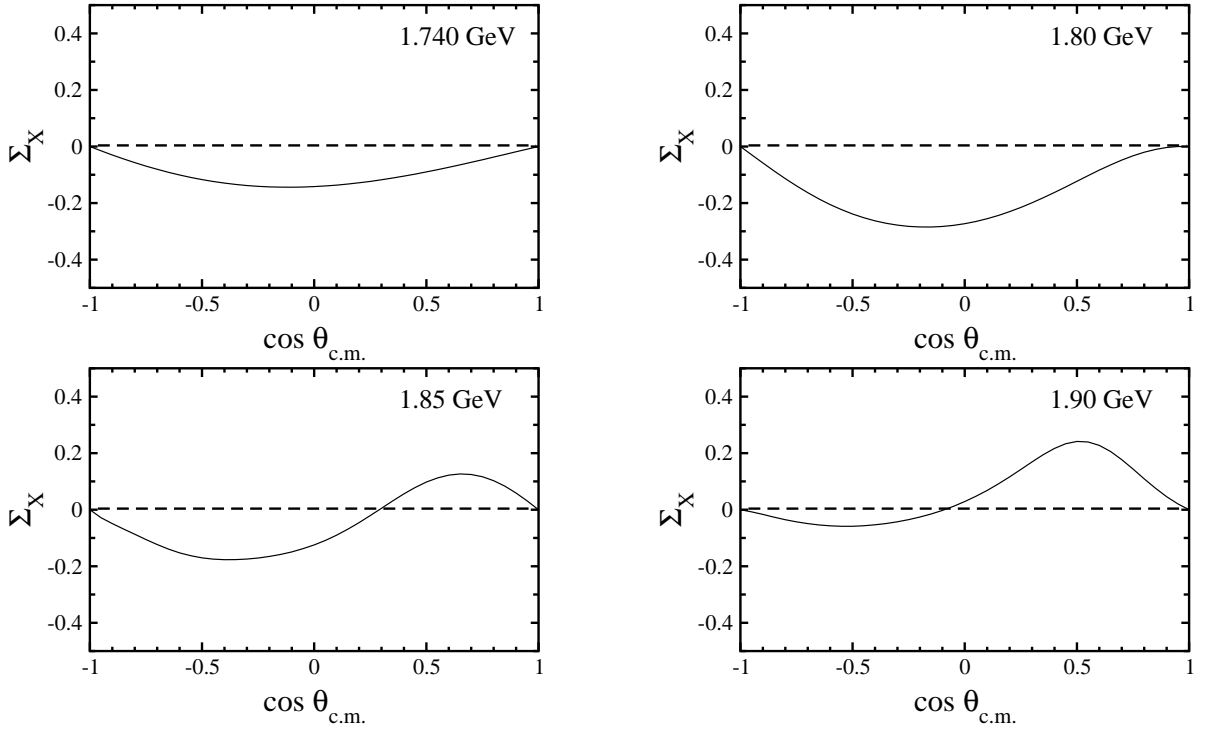


FIG. 13: Photon beam asymmetry  $\Sigma_X$  at fixed energies as a function of the  $\omega$  production angle.

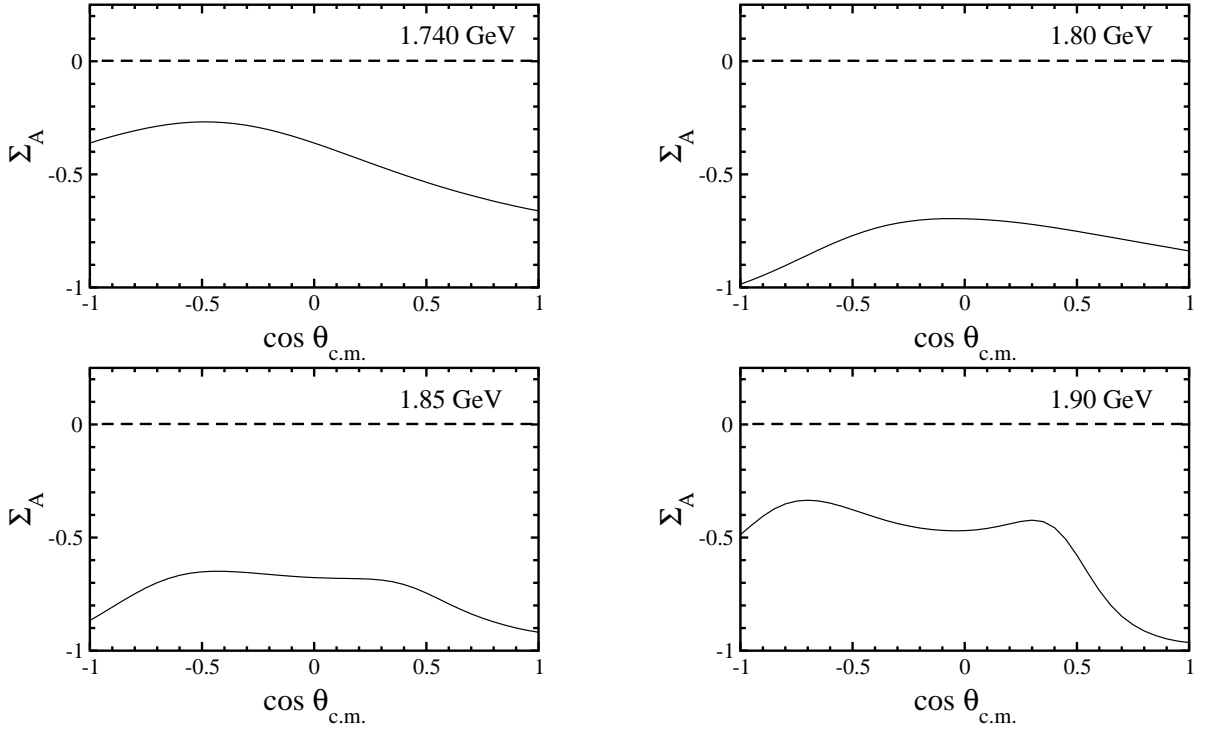


FIG. 14: Photon beam asymmetry  $\Sigma_A$  at fixed energies as a function of the  $\omega$  production angle.

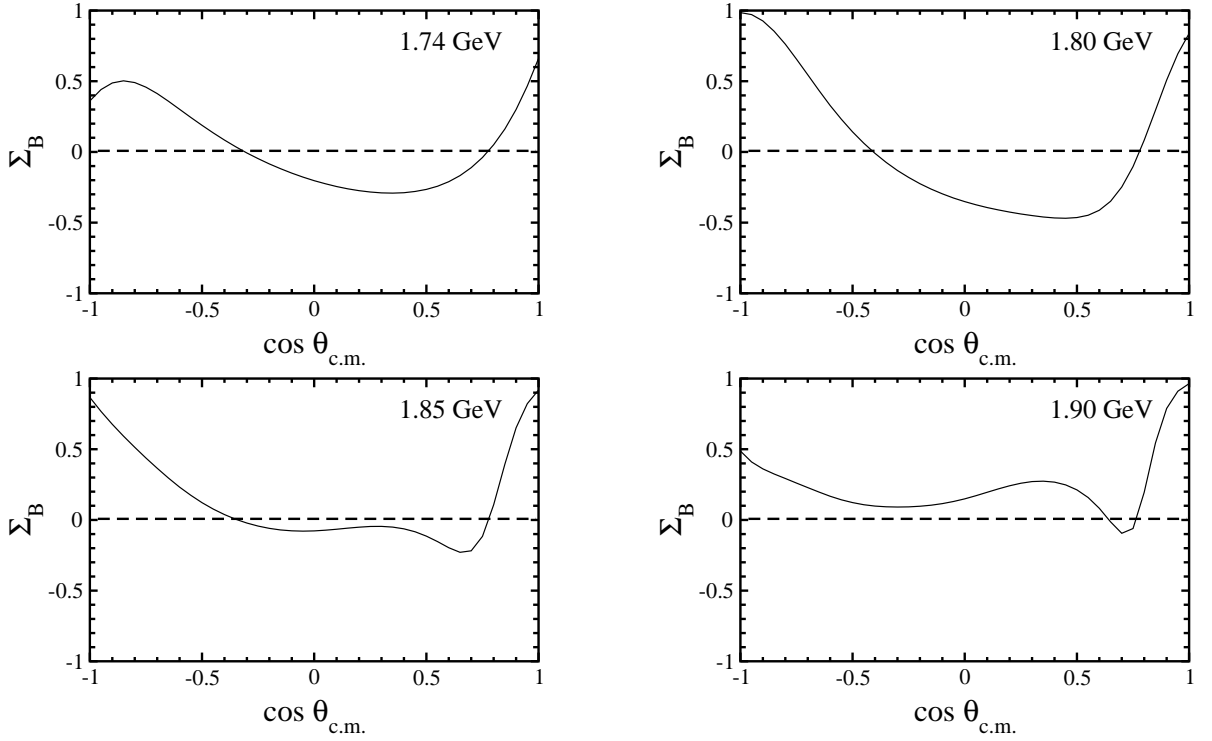


FIG. 15: Photon beam asymmetry  $\Sigma_B$  at fixed energies as a function of the  $\omega$  production angle.

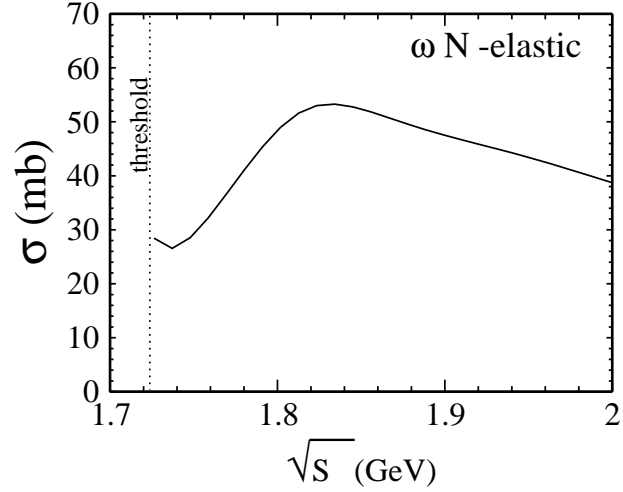


FIG. 16: Elastic  $\omega N$  scattering calculated in the present study.

rather wide energy range. Since the resonance  $\omega N$  couplings are constrained by the  $\pi N \rightarrow \omega N$  and  $\gamma N \rightarrow \omega N$  data, the extracted scattering lengths might suffer from the lack of experimental information at the  $\omega N$  threshold.

## VI. SUMMARY

In the present study we perform a new analysis of the  $\omega$  meson production in  $\pi N$  and  $\gamma N$  reactions within a unitary effective Lagrangian coupled-channel formalism. We have investigated contributions to the  $\omega N$  final state from all spin- $\frac{1}{2}$ ,  $-\frac{3}{2}$ , and spin- $\frac{5}{2}$  resonances with masses below 2 GeV. To fix the resonance couplings a coupled-channel

calculation has been carried out for the final states  $(\gamma/\pi)N \rightarrow \gamma N, \pi N, 2\pi N, \eta N$ , and  $\omega N$  where free parameters of the model are constrained by the all available experimental reaction data for energies from the pion threshold and up to 2 GeV. The extracted resonance couplings to  $\gamma N, \pi N, 2\pi N$ , and  $\eta N$  are found in a good agreement with the results from other analyses and PDG.

Because of the inclusion of the spin- $\frac{5}{2}$  resonance contributions we obtain a significantly better description of the  $\omega$  photoproduction data as compared to our previous calculations. The experimental data on the spin density matrix elements  $\rho_{00}, \rho_{10}$ , and  $\rho_{1-1}$  measured by SAPHIR, give important constraints on the  $\omega$  meson production mechanism. We find a strong contribution from the  $D_{15}(1675)$  resonance to the  $\omega N$  final state in the pion- and photon-induced reactions. While the  $F_{15}(1680)$  state hardly influences the  $\pi N \rightarrow \omega N$  process the contribution from this resonance to the  $\omega$  meson photoproduction turns out to be significant due to its large  $A_{\frac{3}{2}}^p$  helicity amplitude. A strong contribution to the  $\omega$  photoproduction comes from the  $D_{13}$  partial wave which is dominated by the  $\pi^0$  exchange. The effect from the  $D_{13}(1520)$  and  $D_{13}(1950)$  states in this reaction is of minor importance.

Apart from the  $D_{15}(1675)$  and  $F_{15}(1680)$  resonance contributions the  $\omega$  meson photoproduction is strongly dominated by the  $\pi^0$  exchange mechanism which has been also found in the previous findings. We conclude that for the correct description of the experimental data on the  $\omega$  meson production the contribution from the nucleon resonances should be taken into account. However, due to the strong interference pattern between resonances and the  $\pi^0$  exchange the separation of the individual resonance contributions is difficult in this reaction. Hence, a search for 'hidden' resonances with the help of this channel becomes questionable. We predict a negative sign of the photon beam asymmetry in the  $\omega$  photoproduction at energies close to the threshold. Above the 1.85 GeV the  $\Sigma_X$  asymmetry changes its behaviour and becomes positive at the forward angle directions. Since polarization observables, such as  $\rho_{rr'}$  and  $\Sigma_X, \Sigma_A$ , and  $\Sigma_B$  are very sensitive to different reaction mechanisms the more precise measurements of these quantities are urgently needed to distinguish between various model predictions. Our predictions for these observables can easily be checked at GRAAL, CLAS, and CB-ELSA.

## APPENDIX A: COUPLINGS, DECAY WIDTHS, AND HELICITY AMPLITUDES

All interaction Lagrangians for spin- $\frac{1}{2}, \frac{3}{2}$  resonances and Born terms can be found in [2, 3, 5]. Here, we list only those couplings which are extensions of our previous calculations keeping, however, the same notations. The Lagrangians given below contain an isospin part, which is also discussed [2, 3, 5] together with the isospin and partial wave decomposition.

### 1. Tensor meson coupling

The coupling of the tensor  $f_2(1270)$  meson to the nucleon field is described by

$$\mathcal{L}_{NNf_2} = -\bar{u}_{N'}(p') \left[ -i \frac{g_{NNf_2}}{m_N} (\gamma_\mu \bar{\partial}_\nu^{(N'N)} + \gamma_\nu \bar{\partial}_\mu^{(N'N)}) f_2^{\mu\nu} + \frac{h_{NNf_2}}{m_N^2} \bar{\partial}_\mu^{(N'N)} \bar{\partial}_\nu^{(N'N)} f_2^{\mu\nu} \right] u_N(p) \quad (\text{A1})$$

with the asymptotic nucleons  $N, N' = N$ . The notation  $\bar{\partial}_\mu^{(N'N)}$  in the Eq. (A1), related to the nucleon-(tensor)meson  $f^{\mu\nu}$  coupling means  $\bar{\partial}_\mu^{(N'N)} = \partial_\mu^{(N)} - \partial_\mu^{(N')}$  where  $\partial_\mu^{(N)}$  is a derivative over the nucleon field. Such a definition leads to the same transition amplitudes as defined in [59, 60].

The decay  $f_2(1270) \rightarrow \pi\pi$  is described by the Lagrangian

$$\mathcal{L}_{f_2\pi\pi} = -\frac{2g_{f_2\pi\pi}}{m_{f_2}^2} \partial_\mu \pi \partial_\nu \pi f_2^{\mu\nu}, \quad (\text{A2})$$

which is similar to the form used in [59, 61]. This leads to the vertex function for the  $f_2 \rightarrow \pi\pi$  decay:

$$V_{f_2\pi\pi} = -\frac{g_{f_2\pi\pi}}{m_{f_2}^2} (p_1 - p_2)_\mu (p_1 - p_2)_\nu \xi^{\mu\nu}. \quad (\text{A3})$$

$p_1$  and  $p_2$  are outgoing pion momenta and  $\xi^{\mu\nu}$  is a polarization vector of the tensor meson. Using the spin-2 projection operator (see [62, 63, 64, 65])

$$P_{\mu\nu;\rho\sigma}(p) = -\frac{1}{3} \left( -g_{\mu\nu} + \frac{p_\mu p_\nu}{m_p^2} \right) \left( -g_{\rho\sigma} + \frac{p_\rho p_\sigma}{m_p^2} \right)$$

$$\begin{aligned}
& + \frac{1}{2} \left( -g_{\mu\rho} + \frac{p_\mu p_\rho}{m_p^2} \right) \left( -g_{\nu\sigma} + \frac{p_\nu p_\sigma}{m_p^2} \right) \\
& + \frac{1}{2} \left( -g_{\mu\sigma} + \frac{p_\mu p_\sigma}{m_p^2} \right) \left( -g_{\nu\rho} + \frac{p_\nu p_\rho}{m_p^2} \right).
\end{aligned} \tag{A4}$$

The decay width  $f_2(1270) \rightarrow \pi\pi$  is then given by

$$\Gamma = \frac{g_{f_2\pi\pi}^2}{80\pi} m_f \left( 1 - 4 \frac{m_\pi^2}{m_f^2} \right)^{\frac{5}{2}}. \tag{A5}$$

## 2. Spin- $\frac{5}{2}$ Baryon Resonance Interactions

For practical calculations we adopt the spin- $\frac{5}{2}$  propagator in the form

$$\mathcal{P}^{\mu\nu,\rho\sigma}(p) = \frac{(\not{p} + m_p)}{p^2 - m_p^2 + i\epsilon} P^{\mu\nu,\rho\sigma}(p), \tag{A6}$$

with

$$\begin{aligned}
P^{\mu\nu,\rho\sigma}(p) & = \frac{1}{2}(T^{\mu\rho}T^{\nu\sigma} + T^{\mu\sigma}T^{\nu\rho}) - \frac{1}{5}2T^{\mu\nu}T^{\rho\sigma} \\
& + \frac{1}{10}(T^{\mu\lambda}\gamma_\lambda\gamma_\delta T^{\delta\rho}T^{\nu\sigma} + T^{\nu\lambda}\gamma_\lambda\gamma_\delta T^{\delta\sigma}T^{\mu\rho} + T^{\mu\lambda}\gamma_\lambda\gamma_\delta T^{\delta\sigma}T^{\nu\rho} + T^{\nu\lambda}\gamma_\lambda\gamma_\delta T^{\delta\rho}T^{\mu\sigma}),
\end{aligned} \tag{A7}$$

and

$$T^{\mu\nu} = -g^{\mu\nu} + \frac{p^\mu p^\nu}{m_p^2}, \tag{A8}$$

which has also been used in an analysis of  $K\Lambda$  photoproduction [66].

### a. (Pseudo-)Scalar Meson Decay

The Lagrangian for the positive parity spin- $\frac{5}{2}$  resonance decay to a final nucleon  $N$  and a (pseudo-)scalar meson  $\varphi$  is chosen in the form

$$\mathcal{L}_{\frac{5}{2}N\varphi} = \frac{g_{RN\varphi}}{m_\pi^2} \bar{u}_R^{\mu\nu} \Theta_{\nu\lambda}(a_{RN\varphi}) \begin{pmatrix} -i\gamma_5 \\ 1 \end{pmatrix} u_N \partial_\mu \partial^\lambda \varphi + h.c., \tag{A9}$$

and for the negative-parity resonances

$$\mathcal{L}_{\frac{5}{2}N\varphi} = -\frac{g_{RN\varphi}}{m_\pi^2} \bar{u}_R^{\mu\nu} \Theta_{\nu\lambda}(a_{RN\varphi}) \begin{pmatrix} 1 \\ i\gamma_5 \end{pmatrix} u_N \partial_\mu \partial^\lambda \varphi + h.c., \tag{A10}$$

where the upper (lower) factor corresponds to pseudoscalar (scalar) mesons  $\varphi$ .

The free spin- $\frac{5}{2}$  Rarita-Schwinger symmetric field  $u_R^{\mu\nu}$  obeys the Dirac equation and satisfies the conditions  $\gamma_\mu u_R^{\mu\nu} = \partial_\mu u_R^{\mu\nu} = g_{\mu\nu} u_R^{\mu\nu} = 0$  [67]. The off-shell projector  $\Theta_{\mu\nu}(a)$  is

$$\Theta_{\mu\nu}(a) = g_{\mu\nu} - a\gamma_\mu\gamma_\nu, \tag{A11}$$

where  $a$  is related to the commonly used off-shell parameter  $z$  by  $a = (z + \frac{1}{2})$ .

These couplings lead to the decay width (A9) are

$$\Gamma_{\pm}^{\frac{5}{2}} = f_I \frac{g_{RN\varphi}^2}{30\pi m_\pi^4} k_\varphi^5 \frac{E_N \mp m_N}{\sqrt{s}}. \tag{A12}$$

The upper sign corresponds to the decay of the resonance into a meson with the identical parity and vice versa. The isospin factor  $f_I$  is the same as for spin- $\frac{1}{2}, \frac{3}{2}$  resonances (see [2]).  $k_\varphi$ ,  $E_N$ , and  $m_N$  are the meson momentum, energy and mass of the final nucleon, respectively.

b. *Vector Meson Decay*

The coupling of the spin- $\frac{5}{2}$  resonances to the  $\omega N$  final state is chosen to be

$$\mathcal{L}_{\frac{5}{2}N\omega} = \bar{u}_R^{\mu\lambda} \begin{pmatrix} 1 \\ i\gamma_5 \end{pmatrix} \left( \frac{g_1}{4m_N^2} \gamma^\xi + i \frac{g_2}{8m_N^3} \partial_N^\xi + i \frac{g_3}{8m_N^3} \partial_\omega^\xi \right) (\partial_\xi^\omega g_{\mu\nu} - \partial_\mu^\omega g_{\xi\nu}) u_N \partial_\lambda^\omega \omega^\nu + h.c., \quad (\text{A13})$$

where the upper (lower) factor corresponds to positive (negative) parity resonances and  $\partial_N^\mu$  ( $\partial_\mu^\omega$ ) denotes the partial derivative of the nucleon and the  $\omega$ -meson fields, respectively. Note that, in the spin- $\frac{3}{2}$  case, the couplings are also contracted by an off-shell projector (A11). Similar coupling was also used to describe electromagnetic processes [14, 66, 68]. The couplings (A13) lead to the helicity-decay amplitudes

$$\begin{aligned} A_{\frac{3}{2}}^{\omega N} &= \frac{\sqrt{E_N \pm m_N}}{\sqrt{5m_N}} \frac{k_\omega}{4m_N^2} \left( -g_1(m_N \mp m_R) + g_2 \frac{(m_R E_N - m_N^2)}{2m_N} + g_3 \frac{m_\omega^2}{2m_N^2} \right), \\ A_{\frac{1}{2}}^{\omega N} &= \frac{\sqrt{E_N \pm m_N}}{\sqrt{10m_N}} \frac{k_\omega}{4m_N^2} \left( g_1(m_N \pm (m_R - 2E_N)) + g_2 \frac{(m_R E_N - m_N^2)}{2m_N} + g_3 \frac{m_\omega^2}{2m_N^2} \right), \\ A_0^{\omega N} &= \frac{\sqrt{(E_N \pm m_N)}}{\sqrt{5m_N}} \frac{k_\omega m_\omega}{4m_N^2} \left( g_1 \pm g_2 \frac{E_N}{2m_N} \pm g_3 \frac{(m_R - E_N)}{2m_N} \right), \end{aligned} \quad (\text{A14})$$

with upper (lower) signs corresponding to positive (negative) resonance parity. The lower indices stand for the helicity  $\lambda$  of the final  $\omega N$  state  $\lambda = \lambda_V - \lambda_N$  where we use an abbreviation as follows:  $\lambda = 0 : 0 + \frac{1}{2}$ ,  $\frac{1}{2} : 1 - \frac{1}{2}$ ,  $\frac{3}{2} : 1 + \frac{1}{2}$ .

c. *Radiative decay*

The coupling of the spin- $\frac{5}{2}$  resonances to the  $\gamma N$  final state is chosen to be

$$\mathcal{L}_{\frac{5}{2}N\gamma} = e \bar{u}_R^{\mu\lambda} \begin{pmatrix} 1 \\ i\gamma_5 \end{pmatrix} \left( \frac{g_1}{4m_N^2} \gamma^\nu + i \frac{g_2}{8m_N^3} \partial_N^\nu \right) u_N \partial_\lambda F_{\nu\mu} + h.c., \quad (\text{A15})$$

where the upper (lower) factor corresponds to positive (negative) parity resonances. Note that, both couplings are also contracted by an off-shell projector (A11). Similar coupling was also used to describe electromagnetic processes [14, 66, 68].

The electromagnetic helicity amplitudes, which are normalized by an additional factor  $(2E_\gamma)^{-\frac{1}{2}}$  [69], are extracted:

$$\begin{aligned} A_{\frac{1}{2}}^{\gamma N} &= + \frac{e\xi_R}{8m_N^2} \frac{\sqrt{m_R^2 - m_N^2}}{\sqrt{5m_N}} \left( \frac{m_R^2 - m_N^2}{2m_R} \right) \left( g_1 \frac{m_N}{m_R} + g_2 \frac{m_R \pm m_N}{4m_N} \right), \\ A_{\frac{3}{2}}^{\gamma N} &= + \frac{e\xi_R}{4m_N^2} \frac{\sqrt{m_R^2 - m_N^2}}{\sqrt{10m_N}} \left( \frac{m_R^2 - m_N^2}{2m_R} \right) \left( g_1 + g_2 \frac{m_N \pm m_R}{4m_N} \right), \end{aligned} \quad (\text{A16})$$

for spin- $\frac{5}{2}$  resonances. The upper (lower) sign corresponds to positive (negative) parity resonances.  $\xi_R$  denotes the phase at the  $RN\pi$  vertex. The lower indices correspond to the  $\gamma N$  helicities and are determined by the  $\gamma$  and nucleon helicities:  $\frac{1}{2}$ :  $\lambda_\gamma - \lambda_N = 1 - \frac{1}{2} = \frac{1}{2}$  and  $\frac{3}{2}$ :  $1 + \frac{1}{2} = \frac{3}{2}$ .

### 3. off-shell parameters

The off-shell parameters used at the interaction vertices are shown in Table VI. To reduce a number of free parameters of the model we use one overall off-shell parameter for the  $R^{\frac{5}{2}}N\omega$  couplings, so that  $a_{\omega N 3} = a_{\omega N 2} = a_{\omega N 1}$ .

## APPENDIX B: OBSERVABLES

### 1. Spin density matrix

The spin density matrix of the final  $\omega$  mesons produced in the unpolarized  $\gamma N \rightarrow \omega N$  reaction is written as follows:

$L_{2I,2S}$	$a_{\gamma_1}$	$a_{\gamma_2}$	$a_{\pi N}$	$a_{\zeta N}$	$a_{\eta N}$	$a_{\omega N_1}$	$a_{\omega N_2}^b$	$a_{\omega N_3}^b$
$P_{13}(1720)$	2.000	-1.273	-0.650	0.581	2.000	1.404	-1.000	0.951
$P_{13}(1900)$	-3.480	-0.998	-2.000	0.643	1.977	2.537	-2.000	1.483
$D_{13}(1520)$	0.566	0.811	0.007	0.803	0.687	-1.000	2.000	2.000
$D_{13}(1950)$	1.389	1.440	-0.238	0.069	-2.000	0.529	-1.999	0.108
$D_{15}(1675)$	0.882	1.000	0.313	0.198	-1.500	1.398	—	—
$F_{15}(1680)$	0.408	0.955	0.179	0.006	0.387	-0.851	—	—
$F_{15}(2000)$	1.000	0.089	1.697	-0.426	0.999	-0.545	—	—

TABLE VI: Off-shell parameters  $a$  of the spin- $\frac{3}{2}, \frac{5}{2}$  resonances.  $^b$ :  $a_{\omega N_3} = a_{\omega N_2} = a_{\omega N_1}$  for spin- $\frac{5}{2}$  resonances.

$$\rho_{\lambda_\omega \lambda'_\omega}^0 = \frac{\sum_{\lambda_N, \lambda_{N'}, \lambda_\gamma} T_{\lambda_\omega \lambda_{N'}, \lambda_\gamma \lambda_N} T_{\lambda'_\omega \lambda_{N'}, \lambda_\gamma \lambda_N}^*}{\sum_{\lambda_N, \lambda_{N'}, \lambda_\gamma \lambda_\omega} T_{\lambda_\omega \lambda_{N'}, \lambda_\gamma \lambda_N} T_{\lambda'_\omega \lambda_{N'}, \lambda_\gamma \lambda_N}^*}. \quad (B1)$$

$\lambda_N, \lambda_{N'} = \pm \frac{1}{2}$  stand for the helicity of the initial and final nucleon.  $\lambda_\omega = \pm 1, 0$  and  $\lambda_\gamma = \pm 1$  correspond to the  $\omega$  meson and photon helicity respectively. For polarized reactions one can define

$$\rho_{\lambda_\omega \lambda'_\omega}^1 = \frac{\sum_{\lambda_N, \lambda_{N'}, \lambda_\gamma} T_{\lambda_\omega \lambda_{N'}, -\lambda_\gamma \lambda_N} T_{\lambda'_\omega \lambda_{N'}, \lambda_\gamma \lambda_N}^*}{\sum_{\lambda_N, \lambda_{N'}, \lambda_\gamma \lambda_\omega} T_{\lambda_\omega \lambda_{N'}, \lambda_\gamma \lambda_N} T_{\lambda'_\omega \lambda_{N'}, \lambda_\gamma \lambda_N}^*}. \quad (B2)$$

## 2. Beam asymmetry for the $\omega$ photoproduction

The photon beam asymmetry for the meson photoproduction reactions is defined as

$$\Sigma_X = \frac{d\sigma_\perp - d\sigma_\parallel}{d\sigma_\perp + d\sigma_\parallel}, \quad (B3)$$

where  $d\sigma_\parallel$  ( $d\sigma_\perp$ ) is a differential cross section of the  $\gamma p \rightarrow \omega p$  reaction with linearly polarized photons in horizontal (vertical) direction relative to the  $\omega N$  production plane:

$$\begin{aligned} \xi_\parallel = \xi_x &= \frac{-1}{\sqrt{2}}(\xi_{+1} - \xi_{-1}) \\ \xi_\perp = \xi_y &= \frac{i}{\sqrt{2}}(\xi_{+1} + \xi_{-1}). \end{aligned} \quad (B4)$$

The coordinate system is defined by  $\mathbf{z} = \mathbf{k}/|\mathbf{k}|$ ,  $\mathbf{y} = \mathbf{k} \times \mathbf{k}'/|\mathbf{k} \times \mathbf{k}'|$ , where  $\mathbf{k}(\mathbf{k}')$  is a photon(meson) three-momentum. The following asymmetries can be also defined to test the reaction amplitude

$$\begin{aligned} \Sigma_A &= \frac{\rho_{11}^1 + \rho_{1-1}^1}{\rho_{11}^0 + \rho_{1-1}^0}, \\ \Sigma_B &= \frac{\rho_{11}^1 - \rho_{1-1}^1}{\rho_{11}^0 - \rho_{1-1}^0}. \end{aligned} \quad (B5)$$

The differences between  $\Sigma_A$  and  $\Sigma_B$  can be seen on the example of the single  $\pi^0$  exchange mechanism (see below).

## 3. Single $\pi^0$ exchange contribution to the $\omega$ photoproduction.

In the case of the single  $\pi^0$  exchange contribution corresponding to the (c) diagram in Fig. (1) the asymmetry and spin density matrix of the  $\gamma p \rightarrow \omega p$  reaction can be easily calculated. The coupling for the  $\omega \rightarrow \gamma \pi^0$  decay is

proportional to

$$\mathcal{L}_{\omega\gamma\pi^0} \sim \varepsilon_{\mu\nu\rho\sigma} F^{\mu\nu} \partial^\rho \omega^\sigma \pi, \quad (\text{B6})$$

where  $\omega^\sigma(\pi)$ , and  $F^{\mu\nu}$  stand for the vector meson(pion) field and the electromagnetict tensor respectively.  $\varepsilon_{\mu\nu\rho\sigma}$  is a Levi-Chivita tenzor. Then the amplitude of the reaction can be written as

$$\xi_\nu^\gamma \xi_\sigma^\omega J^{\nu\sigma} \sim \varepsilon_{\mu\nu\rho\sigma} k^\mu q^\rho D_\pi(p-p') M(p, p', s_N, s_{N'}), \quad (\text{B7})$$

where  $p(s_N)$  and  $p'(s_{N'})$  are the four momentum(spin) of the initial and final nucleon respectively and  $k, q$  are the photon and vector meson four momenta. The polarization vectors of the photon and vector meson are

$$\xi_{\pm 1}^\mu = \frac{\mp 1}{\sqrt{2}} (\xi_x^\mu \pm i \xi_y^\mu), \quad (\text{B8})$$

for  $\lambda_\gamma, \lambda_\omega = \pm 1$  and

$$\xi_0^\mu = \xi_z^\mu \quad (\text{B9})$$

for longitudinally polarized  $\omega$  mesons. From Eqs. (B1-B5) it follows that only the current

$$J_{\mu\sigma} = \varepsilon_{\mu\nu\rho\sigma} k^\mu q^\rho \quad (\text{B10})$$

in Eq. (B7) contributes to the spin density matrix and asymmetry. Then the final expressions for the spin density matrices are:

$$\begin{aligned} \rho_{\lambda_\omega \lambda_{\omega'}}^0 &= -\frac{1}{2} \left( \frac{m_\omega^2 (k \xi_{\lambda_\omega}^*)(k \xi_{\lambda_{\omega'}})}{(kq)^2} + (\xi_{\lambda_\omega}^* \xi_{\lambda_{\omega'}}) \right), \\ \rho_{\lambda_\omega \lambda_{\omega'}}^1 &= \rho_{\lambda_\omega \lambda_{\omega'}}^0 - \xi_{\lambda_\omega}^{\mu*} \xi_{\lambda_{\omega'}}^\nu \delta_{\mu,2} \delta_{\nu,2}. \end{aligned} \quad (\text{B11})$$

From (B10) and (B11) one deduces that the single  $\pi^0$  exchange contribution in the helicity frame leads to  $\Sigma=0$ ,  $\Sigma_A=-1$ , and  $\Sigma_B=+1$ .

In the Gottfried-Jackson frame defined as a center of mass system of the incoming photon and the exchange pion where the quantization axis is aligned with a photon momentum, the spin density matrix elements given by (B11) becomes  $\rho_{11}^{0,GJ} = \rho_{-1-1}^{0,GJ} = \frac{1}{2}$  and  $\rho_{00}^{0,GJ} = 0$ .

### APPENDIX C: $\omega N$ SCATTERING LENGTHS AND EFFECTIVE RANGES

The spin averaged  $\omega N$  scattering lengths and effective ranges are calculated using the convention of Lutz *et al* [21]:

$$\begin{aligned} \bar{a} &= \frac{1}{3} \bar{a}(J = \frac{1}{2}) + \frac{2}{3} \bar{a}(J = \frac{3}{2}), \\ \bar{r} &= \frac{1}{3} \bar{r}(J = \frac{1}{2}) + \frac{2}{3} \bar{r}(J = \frac{3}{2}). \end{aligned} \quad (\text{C1})$$

The  $\omega N$  helicity state combinations at threshold are [21]

$$\begin{aligned} |\omega N; J = \frac{1}{2}\rangle &= |\omega N, \frac{1}{2}; J = \frac{1}{2}\rangle + \frac{1}{\sqrt{2}} |\omega N, +0; J = \frac{1}{2}\rangle, \\ |\omega N; J = \frac{3}{2}\rangle &= |\omega N, \frac{3}{2}; J = \frac{3}{2}\rangle + \frac{1}{\sqrt{3}} |\omega N, \frac{1}{2}; J = \frac{3}{2}\rangle + \sqrt{\frac{2}{3}} |\omega N, +0; J = \frac{3}{2}\rangle. \end{aligned} \quad (\text{C2})$$

- 
- [1] S. Capstick and W. Roberts, Prog. Part. Nucl. Phys. **45**, S241 (2000), nucl-th/0008028.
- [2] G. Penner and U. Mosel, Phys. Rev. **C66**, 055211 (2002), nucl-th/0207066.
- [3] G. Penner and U. Mosel, Phys. Rev. **C66**, 055212 (2002), nucl-th/0207069.
- [4] G. Penner and U. Mosel, Phys. Rev. **C65**, 055202 (2001), nucl-th/0111023.
- [5] G. Penner, PhD thesis (in English), Giessen, 2002, available via <http://theorie.physik.uni-giessen.de>.
- [6] T. Feuster and U. Mosel, Phys. Rev. **C58**, 457 (1998), nucl-th/9708051.
- [7] T. Feuster and U. Mosel, Phys. Rev. **C59**, 460 (1999), nucl-th/9803057.
- [8] V. Shklyar, G. Penner, and U. Mosel, Eur. Phys. J. **A21**, 445 (2004), nucl-th/0403064.
- [9] J. Barth *et al.*, Eur. Phys. J. **A18**, 117 (2003).
- [10] Q. Zhao, Z.-p. Li, and C. Bennhold, Phys. Rev. **C58**, 2393 (1998), nucl-th/9806100.
- [11] Q. Zhao, Phys. Rev. **C63**, 025203 (2001), nucl-th/0010038.
- [12] Y. Oh, A. I. Titov, and T. S. H. Lee, Phys. Rev. **C63**, 025201 (2001), nucl-th/0006057.
- [13] H. Babacan, T. Babacan, A. Gokalp, and O. Yilmaz, Eur. Phys. J. **A13**, 355 (2002), nucl-th/0108027.
- [14] A. I. Titov and T. S. H. Lee, Phys. Rev. **C66**, 015204 (2002), nucl-th/0205052.
- [15] B. Friman and M. Soyeur, Nucl. Phys. **A600**, 477 (1996), nucl-th/9601028.
- [16] S. Capstick, Phys. Rev. **D46**, 2864 (1992).
- [17] S. Capstick and W. Roberts, Phys. Rev. **D49**, 4570 (1994), nucl-th/9310030.
- [18] R. G. Moorhouse, Phys. Rev. Lett. **16**, 772 (1966).
- [19] Particle Data Group, K. Hagiwara *et al.*, Phys. Rev. **D66**, 010001 (2002), <http://pdg.lbl.gov>.
- [20] S. Capstick, talk given at the NSTAR04, Grenoble, France, 24-27 March 2004.
- [21] M. F. M. Lutz, G. Wolf, and B. Friman, Nucl. Phys. **A706**, 431 (2002), nucl-th/0112052.
- [22] Y. Oh and T. S. H. Lee, Nucl. Phys. **A721**, 743 (2003), nucl-th/0211054.
- [23] Y. Oh and T. S. H. Lee, Phys. Rev. **C66**, 045201 (2002), nucl-th/0204035.
- [24] A. D. Lahiff and I. R. Afnan, Phys. Rev. **C60**, 024608 (1999), nucl-th/9903058.
- [25] R. J. Yaes, Phys. Rev. **D3**, 3086 (1971).
- [26] F. Gross and Y. Surya, Phys. Rev. **C47**, 703 (1993).
- [27] Y. Surya and F. Gross, Phys. Rev. **C53**, 2422 (1996).
- [28] B. C. Pearce and B. K. Jennings, Nucl. Phys. **A528**, 655 (1991).
- [29] P. F. A. Goudsmit, H. J. Leisi, E. Matsinos, B. L. Birbrair, and A. B. Gridnev, Nucl. Phys. **A575**, 673 (1994).
- [30] E. Oset and A. Ramos, Nucl. Phys. **A635**, 99 (1998), nucl-th/9711022.
- [31] T. Sato and T. S. H. Lee, Phys. Rev. **C54**, 2660 (1996), nucl-th/9606009.
- [32] O. Krehl, C. Hanhart, S. Krewald, and J. Speth, Phys. Rev. **C62**, 025207 (2000), nucl-th/9911080.
- [33] C. Schutz, J. Haidenbauer, J. Speth, and J. W. Durso, Phys. Rev. **C57**, 1464 (1998).
- [34] J. Speth, O. Krehl, S. Krewald, and C. Hanhart, Nucl. Phys. **A680**, 328 (2000).
- [35] N. Kaiser, T. Waas, and W. Weise, Nucl. Phys. **A612**, 297 (1997), hep-ph/9607459.
- [36] J. Caro Ramon, N. Kaiser, S. Wetzel, and W. Weise, Nucl. Phys. **A672**, 249 (2000), nucl-th/9912053.
- [37] R. M. Davidson and R. Workman, Phys. Rev. **C63**, 025210 (2001).
- [38] D. M. Manley, R. A. Arndt, Y. Goradia, and V. L. Teplitz, Phys. Rev. **D30**, 904 (1984).
- [39] D. M. Manley and E. M. Saleski, Phys. Rev. **D45**, 4002 (1992).
- [40] T. P. Vrana, S. A. Dytman, and T. S. H. Lee, Phys. Rept. **328**, 181 (2000), nucl-th/9910012.
- [41] R. A. Arndt, I. I. Strakovsky, R. L. Workman, and M. M. Pavan, Phys. Rev. **C52**, 2120 (1995), nucl-th/9505040.
- [42] R. A. Arndt, R. L. Workman, I. I. Strakovsky, and M. M. Pavan, Phys. Scr. **T87**, 62 (2000), nucl-th/9807087.
- [43] C. Deutsch-Sauermann, B. Friman, and W. Norenberg, Phys. Lett. **B409**, 51 (1997), nucl-th/9701022.
- [44] C. Sauermann, B. L. Friman, and W. Norenberg, Phys. Lett. **B341**, 261 (1995), nucl-th/9408012.
- [45] R. Machleidt, K. Holinde, and C. Elster, Phys. Rept. **149**, 1 (1987).
- [46] F. Gross, J. W. Van Orden, and K. Holinde, Phys. Rev. **C45**, 2094 (1992).
- [47] J. Barth *et al.*, Eur. Phys. J. **A18**, 117 (2003).
- [48] R. A. Arndt, W. J. Briscoe, I. I. Strakovsky, R. L. Workman, and M. M. Pavan, Phys. Rev. **C69**, 035213 (2004), nucl-th/0311089.
- [49] R. A. Arndt, I. I. Strakovsky, and R. L. Workman, Phys. Rev. **C53**, 430 (1996), nucl-th/9509005; R. A. Arndt, W. J. Briscoe, I. I. Strakovsky, and R. L. Workman, Phys. Rev. **C66**, 055213 (2002), nucl-th/0205067.
- [50] M. Batinic, I. Slaus, A. Svarc, and B. M. K. Nefkens, Phys. Rev. **C51**, 2310 (1995), nucl-th/9501011, Erratum-ibid. **C57**:1004,(1998).
- [51] G.-Y. Chen, S. Kamalov, S. N. Yang, D. Drechsel, and L. Tiator, Nucl. Phys. **A723**, 447 (2003), nucl-th/0210013.
- [52] R. E. Cutkosky and S. Wang, Phys. Rev. **D42**, 235 (1990).
- [53] G. Hohler, F. Kaiser, R. Koch, and E. Pietarinen.
- [54] H. Karami *et al.*, Nucl. Phys. **B154**, 503 (1979).
- [55] J. S. Danburg *et al.*, Phys. Rev. **D2**, 2564 (1970).
- [56] D. M. Binnie *et al.*, Phys. Rev. **D8**, 2789 (1973).
- [57] J. Keyne *et al.*, Phys. Rev. **D14**, 28 (1976).
- [58] F. Klingl, T. Waas, and W. Weise, Nucl. Phys. **A650**, 299 (1999), hep-ph/9810312.

- [59] H. Pilkuhn *et al.*, Nucl. Phys. **B65**, 460 (1973).
- [60] H. Goldberg, Phys. Rev. **171**, 1485 (1968).
- [61] Y.-s. Oh and T. S. H. Lee, Phys. Rev. **C69**, 025201 (2004), nucl-th/0306033.
- [62] D. H. Sharp and W. G. Wagner, Phys. Rev. **131**, 2226 (1963).
- [63] S. Weinberg, Phys. Rev. **133**, B1318 (1964).
- [64] S. Bellucci, J. Gasser, and M. E. Sainio, Nucl. Phys. **B423**, 80 (1994), hep-ph/9401206.
- [65] D. Toublan, Phys. Rev. **D53**, 6602 (1996), hep-ph/9509217.
- [66] J. C. David, C. Fayard, G. H. Lamot, and B. Saghai, Phys. Rev. **C53**, 2613 (1996).
- [67] W. Rarita and J. S. Schwinger, Phys. Rev. **60**, 61 (1941).
- [68] M. Zetenyi and G. Wolf, Phys. Rev. **C67**, 044002 (2003), nucl-th/0103062.
- [69] M. Warns, H. Schroder, W. Pfeil, and H. Rollnik, Z. Phys. **C45**, 627 (1990).